



VIENNA
UNIVERSITY OF
TECHNOLOGY

INSTITUTE OF
PHOTOGRAMMETRY
AND REMOTE SENSING

DIPLOMARBEIT

Performance evaluation of a Range Camera SR4000

Ausgeführt am Institut für
Photogrammetrie und Fernerkundung
der Technischen Universität Wien

unter der Anleitung von
Univ.Prof. Dipl.-Ing. Dr.techn. Norbert Pfeifer

durch

ALEXANDRA VON BERINGE

Matrikelnummer: 0425512

Görgengasse 23/3/6

1190 Wien

Wien, im Juni 2012

Diese Diplomarbeit möchte ich meinen Eltern Sylvia und Niklas von Beringe widmen. Sie haben mir nicht nur mein Studium ermöglicht, sondern mich auch stets mit Rat und Tat unterstützt. Besonders in Zeiten, in denen ich mit dieser Diplomarbeit eher kleine als große Fortschritte gemacht habe, konnten sie mich immer zum Weitermachen motivieren.

Abstract

This thesis deals with a performance evaluation of a range camera SR4000. Range cameras represent a young technology and their measurement method offers an essential advantage: Masses of points can be determined simultaneously by runtime measurement. The measurements of a range camera are impaired by various factors of influence though. Hence, the reliability of the measurements and the measurement accuracy are restricted.

Four different factors of influence and their impacts on the camera's measurements are in the focus of this thesis. Four different tests have hence been performed with two targets which have a very different reflectivity of 10% and 99%, respectively. By analysing the distance measurements and the amplitude measurements of the camera, statements on the camera's performance can be made.

First, the process of the measurements during the warm up time is investigated. As the camera warms up during the use and especially needs some time in the beginning of a data acquisition to achieve a stable performance, this specific factor of influence is in the focus of analysis in order to specify a certain warm up period.

The second test concentrates on the observed distances as changing the distances between camera and object affects the camera's measurements. A functional model is presented to provide information on the distance measurement accuracy.

Third, variations of the integration time are examined. The integration time is a very important factor as it defines how long each sensor pixel collects light. Furthermore, different integration times cause different measurement results. The extent of these differences is investigated here.

The fourth test deals with the background light as influencing factor. Although the camera has an integrated optical filter which prevents background light from reaching the sensor, some light still gets through and impairs the camera's measurements.

The last part of this thesis addresses the performed reference survey. The distances between camera and object were determined with the range camera on the one hand and with a total station on the other hand. Here, the outcomes are compared.

Zusammenfassung

Diese Diplomarbeit befasst sich mit der Leistungseinschätzung einer Distanzkamera SR4000. Distanzkameras sind eine relativ junge Technologie, deren Messmethode einen entscheidenden Vorteil hat: Massenweise Punktbestimmung basierend auf Laufzeitmessung. Die Messungen einer Distanzkamera werden jedoch durch verschiedenste Einflussfaktoren beeinträchtigt. Dadurch ist die Zuverlässigkeit der Messungen und deren Messgenauigkeit eingeschränkt.

Vier verschiedene Einflussfaktoren und ihre Auswirkungen auf die Messungen der Kamera stehen im Mittelpunkt dieser Diplomarbeit. Vier unterschiedliche Tests wurden daher durchgeführt, basierend auf zwei Zielobjekten, die stark unterschiedliche Reflektivitäten aufweisen (10% bzw. 99%). Durch die Analyse der gewonnenen Distanz- und Amplitudenmessungen, können Schlüsse betreffend der Messleistung der Kamera gezogen werden. Zunächst wird das Aufwärmverhalten der Kamera untersucht. Da sich die Kamera während der Verwendung erwärmt und vor allem am Anfang einer Datenaufnahme eine gewisse Zeit benötigt um stabile Messungen zu liefern, wird genau dieser Zeitfaktor hier analysiert, um am Ende eine bestimmte Aufwärmzeit definieren zu können.

Der zweite Test konzentriert sich auf die Beobachtungsdistanzen, da Änderungen der Distanzen zwischen Kamera und Objekt die Messungen beeinflussen. Ein funktionales Modell wird vorgestellt, mit dem Aussagen über die Messgenauigkeit der Distanzmessungen getroffen werden können.

Zum Dritten werden Änderungen der Integrationszeit untersucht. Die Integrationszeit stellt einen sehr wichtigen Faktor dar, da sie den Zeitraum festlegt, in dem jedes Pixel Licht aufnimmt. Unterschiedliche Integrationszeiten verursachen zudem Unterschiede in den Ergebnissen der Distanzmessung. Das Ausmaß der auftretenden Differenzen wird hier untersucht.

Der vierte Test widmet sich dem Hintergrundlicht. Obwohl in die Kamera ein optischer Filter integriert ist, dringt trotzdem eine gewisse Menge an Licht zu dem Sensor durch und beeinträchtigt die Messresultate.

Der letzte Teil dieser Diplomarbeit beschäftigt sich mit der Referenzvermessung. Die Distanzen zwischen Kamera und Objekt wurden auf der einen Seite mit der Distanzkamera und auf der anderen Seite mit einer Totalstation bestimmt. Die Ergebnisse der Messungen werden hier verglichen.

Contents

1	Introduction	1
1.1	Motivation	1
1.2	Related work	2
1.3	Outline of the thesis	3
2	Fundamentals	4
2.1	Time-of-Flight principle	5
2.1.1	Pulse Modulation	6
2.1.2	Continuous Wave (CW) Modulation	7
2.2	Range Imaging technology	9
2.3	Details of the investigated camera	10
3	Experiments	12
3.1	Environment of the experiments	12
3.1.1	Spectralon Targets	13
3.1.2	Software	14
3.1.3	Reference Survey	17
3.1.4	Operating the camera	20
3.2	Warm Up Test	21
3.2.1	Task	21
3.2.2	Observation objects	21
3.2.3	Variables	21
3.2.4	Data acquisition and preprocessing	22
3.3	Distance Test	25
3.3.1	Task	25
3.3.2	Observation objects	25
3.3.3	Variables	25
3.3.4	Data acquisition and preprocessing	26
3.4	Integration Time Test	29
3.4.1	Task	29
3.4.2	Observation objects	29
3.4.3	Variables	30
3.4.4	Data acquisition and preprocessing	30
3.5	Background Light Test	32
3.5.1	Task	32
3.5.2	Observation objects	33
3.5.3	Variables	33
3.5.4	Data acquisition and preprocessing	34

4	Analysis	37
4.1	Preliminary Processing Measures	37
4.2	Analysis of the Warm Up Test	40
4.2.1	Effects on distance measurements	40
4.2.2	Effects on amplitude measurements	42
4.3	Analysis of the Distance Test	45
4.3.1	Effects on distance measurements	45
4.3.2	Effects on amplitude measurements	53
4.4	Analysis of the Integration Time Test	54
4.4.1	Effects on distance measurements	55
4.4.2	Effects on amplitude measurements	58
4.5	Analysis of the Background Light Test	59
4.5.1	Effects on distance measurements	59
4.5.2	Effects on amplitude measurements	61
4.6	Analysis of the Reference Survey	62
5	Conclusion	66
5.1	Future Work	67
	References	69
	List of Figures	72
	List of Tables	74
A	Appendix	75
A.1	Datasheet Range Camera SR4000	75
A.2	Datasheet Spectralon Targets	84
B	Curriculum Vitae	87

1 Introduction

Since the first realization of an all-solid-state range camera by *Lange* [17] in the year 2000 the technology of range imaging has been passing a rapid development. Several vendors introduced range cameras and further improvements in the last few years. Although range imaging is a relatively young technology, range cameras are now already applied in different fields of work. Medicine, logistics, films and TV and several more branches already use range imaging [11]. Particularly in the automotive industry (e.g. to identify pedestrians) and robotics (e.g. to estimate the motion of a robot) range cameras have already been implemented successfully [22, 30].

Range Imaging (RIM) combines two different and well known technologies: Photogrammetry and laser scanning. Photogrammetry concentrates on simultaneous 3D point measurement with the aim to reconstruct the position and size of 3D objects. Therefore, different exposure positions and the corresponding common points are necessary. With laser scanning 3D points are determined by runtime measurement of laser light. The need for common points is not given with this technology, nevertheless a simultaneous point gathering is not possible as only one distance is determined at a time. With RIM the advantages of both technologies are united as the determination of masses of points is realized through runtime measurement. Also moving scenes can be acquired with this technology.

As the name implies, range imaging comprises distance measurements as well as imaging aspects. This combination is achieved by special types of sensors which allow distance measurements for a whole amount of pixels at the same time. Although there are still various limitations, e.g. in terms of accuracy or operating range, RIM means a valuable enrichment of measuring and modelling technologies.

1.1 Motivation

The first impulse for this master thesis was a research stay within the frame of an exchange semester at the University of Calgary, Canada. Based on the scientific cooperation with Prof. Derek Lichti at the University of Calgary (UofC), Prof. Norbert Pfeifer from the Institute of Photogrammetry and Remote Sensing of the Technical University of Vienna (TU Vienna) supported this sojourn abroad in the fall of 2009.

The Institute at the TU Vienna has got a range camera *Swiss Ranger* SR3000, and the UofC purchased the new model SR4000 just a few months before the

research stay. As many tests and performance evaluations of the SR3000 had already been performed, the SR4000 now posed a new challenge.

The behaviour of any range camera is affected by several factors of influence, e.g. the distance between camera and object. As this new camera, the SR4000, had not been tested often at that time (see section 1.2), these factors were still not known in detail. With unknown influencing factors the accuracy of distance measurements in the range of cm is not accurate enough in terms of geodesy, where accuracies of mm or sub-mm are essential. However, modelling and thereby lowering the influence of these factors would be desirable as the employment of range cameras in surveying tasks in general is highly relevant due to the already mentioned advantages.

This master thesis hence concentrates on the examination and following modelling of several factors of influence to contribute to the increase of distance accuracy, so that the SR4000 can hopefully be employed in surveying tasks in the near future.

1.2 Related work

As mentioned before, one of the first 3D time-of-flight cameras was introduced by *Lange* in 2000 [17]. Here, electronics as well as hardware and pixel concepts of the first realization of an all solid-state range camera are described. In 2004, *Oggier et al.* [23] introduced the new range camera SwissRanger2 (SR2), predecessor of the camera used for this thesis. With the SR2, which was the first commercial model, sub-cm distance precision could be achieved. In 2005, *Oggier et al.* [24] presented the successor model of the SR2, the SwissRangerR3000 (SR3000), and described the first experiences with this camera. *Chiabrando et al.* [4] reported in 2009 on tests with the latest SwissRanger model: The SwissRanger4000 (SR4000), which is also the focus of this work. Probably the most important development of the SR3000 was the implementation of a reference path in the SR4000, which reduces occurring drifts in the distance measurements [8].

During the last years a lot of efforts have been made to improve the performance of range cameras. But still, many factors of influence impair the measurements. *Chiabrando et al.* [4] performed an evaluation of the SR4000 especially in terms of warm up time, integration time and incidence angle. *Weyer et al.* [31] concentrated on integration time and reflectivity among others, the influence of background light was investigated by *Büttgen et al.*

[3]. *Karel et al.* [12] focused on scattering, *Kahlmann et al.* [8] reported on the impacts because of changes in the internal or external temperature and the dependence of the amplitude on the distance. All in all it has to be said that literature on the SR4000 is very scarce. Regarding this camera model, no literature on the influence of amplitudes on range measurements or the influence of background light was available.

1.3 Outline of the thesis

In the following work the range camera *Swiss Ranger* SR4000 and some influencing factors which affect the camera's measurements will be investigated in detail. Chapter 2 will give an overview of the topic range measurement. Different measurement techniques will be described and especially the most relevant principle Time of Flight is dealt with in detail. Additionally, it will be elaborated on the technology and functionality of range imaging. Finally, the second chapter describes the most important details and facts of the applied range camera *Swiss Ranger* SR4000.

Chapter 3 deals with the experiments which were performed in the context of this thesis. Four different factors of influence were examined and are described here. Also the environment of the experiments and the used software are discussed. In addition to the distance measurements of the range camera, the distances were also determined with a total station for comparison. The respective procedure of this reference survey is described here. At last, the preprocessing is depicted and the first results of the experiments are presented.

In chapter 4 the factors of influence are investigated in detail. At first, different adjustment processes are explained before the influencing factors are analysed in detail. Besides that, the last section is concerned with the analysis of the reference survey. Here, the distance measurements gathered with the total station are compared to the distance measurements obtained with the SR4000.

Finally, chapter 5 summarizes the gained results and gives ideas for future work.

2 Fundamentals

Basically, there are various types of contact-free, optical 3D range measurement techniques. The most important principles are triangulation, interferometry and Time-of-Flight. All these techniques work with signals of different wavelengths. Figure 1 gives an introductory overview:

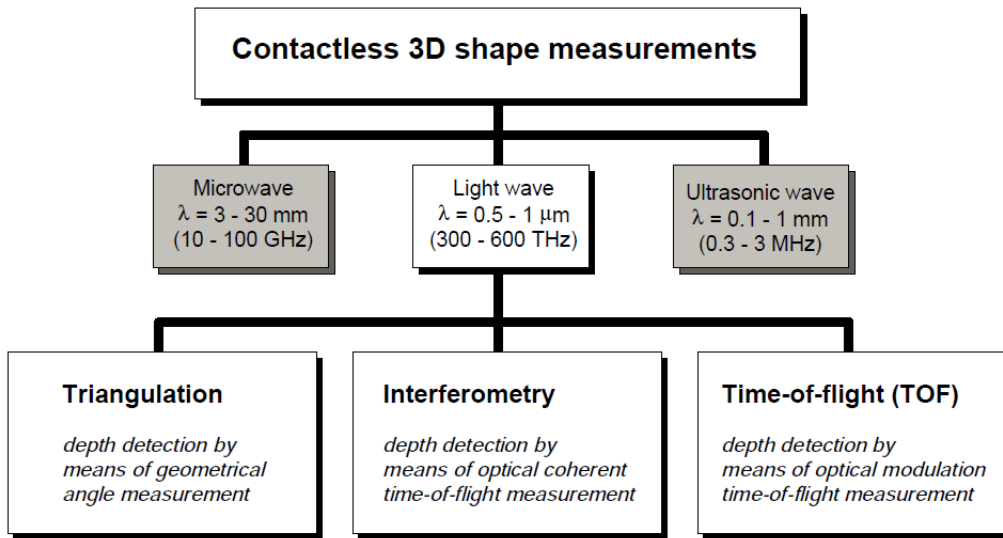


Figure 1 – Overview of contact-less 3D measurements, figure taken from [27], modified by [17]

Microwaves are characterized by long wave lengths of 3 - 30 mm and are used for popular applications like GPS (Global Positioning System) or SAR (Synthetic Aperture Radar) [7, 15, 27]. Ultrasonic waves are mainly applied in underwater surveying [28]. Due to low angular resolution (and accordingly low accuracy) respectively inefficiency in the air (due to low propagation speed of sound in air, which is not sufficient for applications requiring a high frame rate) only light waves are interesting for the mentioned techniques in figure 1 [26].

Triangulation (see figure 2), a geometrical method, is probably the oldest measurement method to determine an unknown distance. The target represents an unknown corner point of a triangle while the coordinates of both other points (A and B in figure 2) are known. By measuring the angles of the triangle respectively the base x between the two known corner points, the horizontal distance z and further the coordinates of the target can be

determined.

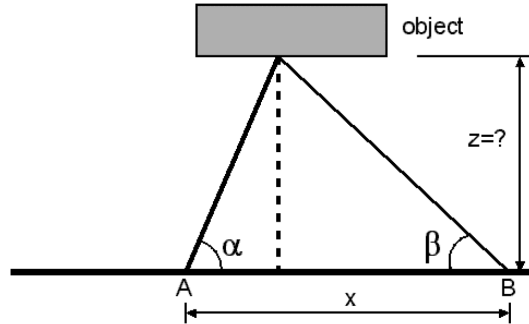


Figure 2 – *Setup of a triangulation [17]*

With interferometry, coherent light (in general laser light) waves are superposed, the distance can be determined by measuring the phase delays. Because of the characteristics of the used light waves this method is also known as coherent Time-of-Flight measurement.

Time-of-Flight is based on the runtime measurement of light. Therefore, either laser (Light Amplification by Stimulated Emission of Radiation) diodes or LEDs (Light Emitting Diodes) are used. Depending on the diodes, either coherent or incoherent Time-of-Flight measurement is applied. Coherent laser light offers a high optical power and is used e.g. in Laser Scanning [14]. With incoherent time of flight measurement, on the other hand, a whole scene gets illuminated by an incoherent light source instead of a laser beam. LEDs are cheaper and often smaller than lasers.

Regardless of whether laser diodes or LEDs are used, the emitted light is modulated with a modulation signal, whose characteristics are used for the determination of the distance. As this measurement method is applied in the observed range camera, it will be explained in more detail in the following chapter. More information on the briefly introduced methods triangulation and interferometry can be found in [1, 6, 17].

2.1 Time-of-Flight principle

The distance measurements of a range camera are based upon the Time-of-Flight (ToF) principle. ToF is a 3D-measuring method which uses travel time measurement to determine distances. Fundamental for this method is the speed of light c , which is known very precisely [2]:

$$c = 299792458 \text{ m/s} \quad (1)$$

Basically, an active illumination source sends out light towards the object of interest, which is then reflected from the object to the sensor. As already mentioned before, the emitted light is modulated by the illumination source and is demodulated again by the light detector when reaching the sensor. The two most common modulation principles are the Pulse Modulation and the Continuous Wave (CW) Modulation.

2.1.1 Pulse Modulation

The Pulse Modulation is drafted in figure 3.

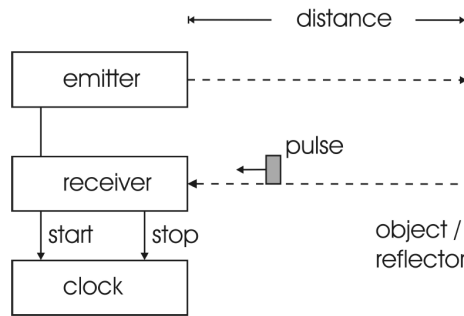


Figure 3 – *Pulse Modulation [32]*

A light pulse is emitted, travels a certain distance to a reflector and after the reflection back to the sensor. When emitting, a high-precision clock starts to run and stops as the pulse is detected again by the receiver. With the given speed of light and the measured time of travel the travelled distance ($2D$) can be calculated as follows:

$$2D = c \cdot t \quad (2)$$

The distance between the camera and the object of interest results then in half of the travelled distance:

$$D = \frac{c \cdot t}{2} \quad (3)$$

with D distance between camera and reflector
 c speed of light
 t time of travel

In order to achieve a high distance-accuracy, the internal clock has to be highly accurate. A time resolution of 67 ps is required to reach a distance resolution of 1 cm [8].

As the travelled time (also called pulse-round-trip-time) is determined directly by a clock in this measuring principle, this method is also called *direct Time-of-Flight* [6, 8, 17].

2.1.2 Continuous Wave (CW) Modulation

With this method, a light wave is continuously modulated in its amplitude. Figure 4 shows the operating principle.

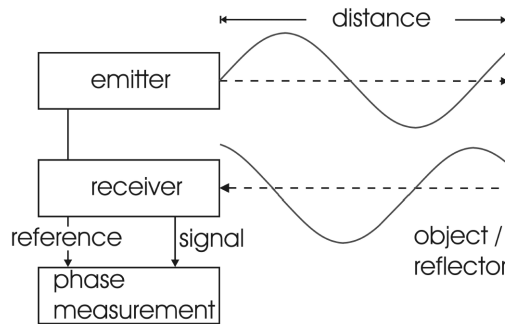


Figure 4 – *Continuous Wave Modulation* [32]

The emitted signal is sinusoidally modulated, scattered back by the object/reflector and is demodulated again by the receiver. The distance can be determined with the phase difference of the emitted and received signal, which means a fraction of a full cycle of the modulated signal. This phase difference is measured by the sensor. The distance for a full cycle is given by

$$L = \frac{c}{2f_{mod}} \quad (4)$$

where f_{mod} is the modulation frequency.

Figure 5 points out the measurement principle in more detail. The also sinusoidally incoming signal is shifted in amplitude A , offset B and phase φ .

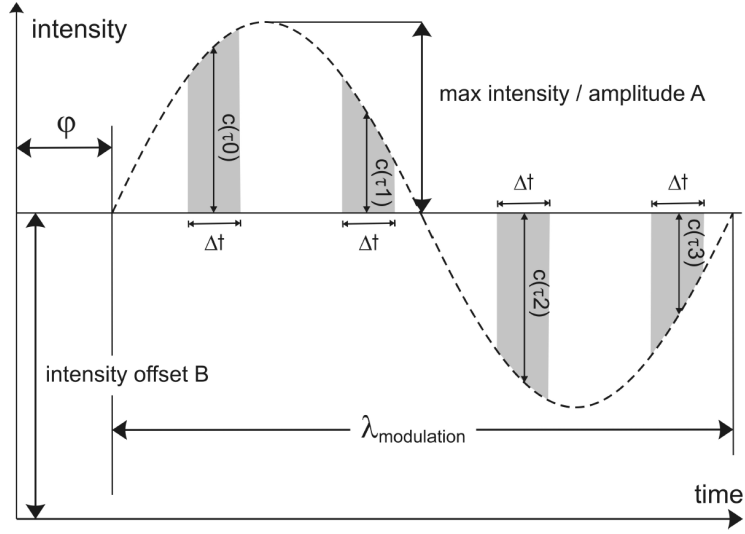


Figure 5 – Phase shift measurement principle [8]

The originally emitted signal (with $\varphi=0$) is not shown in figure 5. The received signal is demodulated by sampling the sinusoidal wave at four sampling points per modulation period: $c(\tau_0)$, $c(\tau_1)$, $c(\tau_2)$ and $c(\tau_3)$. The method to determine these sampling points is based on a correlation of the emitted and received signal - a so-called cross correlation [23]. With the values determined this way, the offset B , amplitude A and phase φ can be calculated (see [17]):

$$B = \frac{c(\tau_0) + c(\tau_1) + c(\tau_2) + c(\tau_3)}{4} \quad (5)$$

$$A = \frac{\sqrt{(c(\tau_0) - c(\tau_2))^2 + (c(\tau_1) - c(\tau_3))^2}}{2} \quad (6)$$

$$\varphi = \arctan \frac{c(\tau_0) - c(\tau_2)}{c(\tau_1) - c(\tau_3)} \quad (7)$$

The amplitude A can be used to create an intensity image and furthermore provides information on the saturation of the sensor. The distance D between sensor and object can be calculated as [4]:

$$D = \frac{c \cdot \varphi}{4\pi \cdot f_{mod}} \quad (8)$$

As the phase differences are used for determining distances rather than the Time-of-Flight, this method is also known as *indirect Time-of-Flight* distance measurement method. More detailed facts on continuous wave modulation can be found in [17] and [8].

The next sub-chapters dwell more specifically on the range camera *Swiss Ranger* SR4000, which was used for this thesis. Section 2.2 gives a short introduction on the range image technology of a SR4000, 2.3 finally covers a detailed description of the SR4000.

2.2 Range Imaging technology

The methods to measure distances as discussed in 2.1.1 and 2.1.2 describe a single distance determination at one point of time as it is already known from e.g. laser scanners. The range imaging technology, however, allows the simultaneous implementation of this method for several distance measurements at the same time. "Range imaging combines the distance measurement technology with the advantages of those of imaging arrays. Simplified, it just enables each pixel to measure the distance towards the corresponding object point." ([9], 137) Here, each pixel represents an own distance measurement system.

As already described in the previous section, the distance determination is achieved by modulation and following demodulation. First, the whole scene is illuminated simultaneously by LEDs. After the emitted light is reflected and arrives at the range camera, it is mapped by optics onto the sensor and thus onto a focal plane array. In the SR4000, the demodulation process is then performed separately in each pixel and is based on a combined CCD/CMOS-process. The pixel architecture is based on so-called lock-in pixels which are described in detail in [3] and [17]. With the calculated distances and simple geometry the 3D coordinates of the object points can be computed [8, 10].

Apart from the combined CCD/CMOS technology, which is used in range cameras of *Mesa Imaging*, another technology for range cameras was developed at about the same time and needs to be mentioned here. This method is based on a complete CMOS-process and is applied in Photonic Mixing

Devices (PMD). Although both technologies have similar backgrounds and hence have many common features, they differ due to their sensor technologies. PMD-cameras are not subject of this thesis and are therefore not described in more detail. [8] and [21] give more information on this technology.

2.3 Details of the investigated camera

The centre of this master thesis is the range camera *Swiss Ranger 4000* (SR4000) of the company *Mesa Imaging*, see figure 6. The handy range camera with the dimensions of 65x65x68 mm has an integrated pixel field of 144x176 pixels and is based on the Continuous Wave modulation (see 2.1.2). As already indicated, the distance is determined at each pixel by means of the phase shift. As to equation 4 and considering the camera's default modulation frequency of 30 MHz (which was not changed during the whole data acquisition of this study) this equation results to the range of a full cycle of 5 m. This distance hence means the maximum unambiguous range of the SR4000.



Figure 6 – *Swiss Ranger SR4000*

An array of 24 LEDs is the active illumination of the range camera. The camera is designed for indoor use and has an optical filter in front of the sensor to allow only wavelengths near that of the illumination LEDs to pass into the camera lens.

Compared to the preceding camera model (SR3000), the SR4000 shows considerable technological improvements. Very important is the internal reference path, which was implemented in the SR4000 for the first time. This path allows the internal synchronisation between the illumination and the sensor. Earlier camera models without this synchronisation feature are more susceptible for temperature changes (which automatically occur when using

the range camera, see 3.2) [8].

Another improvement from the SR3000 to the SR4000 concerns the cooling. In the SR3000 an active cooling system is integrated which is realized with a ventilator. The cooling system of the SR4000 has been changed to a passive cooling. This leads to a more constant operating mode as the ventilator of the SR3000 does not run regularly but is switched on at a certain sensor temperature and thus causes irregularities in the measurements.

One more change is the modulation frequency, which has been increased from 20 mHz to 30 mHz. Thus, a higher distance accuracy can be achieved. The modulation frequency of the SR4000 can be changed in an integer range of ± 1 mHz.

More technical details about the SR4000 are listed in the datasheet (see A.1).

3 Experiments

In order to use this enriching technology of Range Imaging in terms of geodesy and surveying, the accuracy of the measurements has to be improved. A range accuracy of ± 10 mm (see A.1) specified by the manufacturer *Mesa Imaging* is too inaccurate for surveying purposes, where accuracies of mm–sub-mm are required.

To improve the accuracy, it is necessary to learn more about the behaviour of the camera and thus get an evaluation of its performance. This is realised in this study by four separate tests, in which different factors of influence are observed. The warm up time of the camera was examined, the effects of changes in distance between camera and object and in integration time and the influence of background light were observed. These factors of influence will be discussed in detail in the following sections. In addition to the factors already mentioned another focus is turned to the reflectivity of the observed targets.

With these tests and the concluding results statements about the camera's performance and measurement accuracy can be made in the end.

3.1 Environment of the experiments

For each factor of influence an own test sequence was developed, but basically the setups for the four different parts were similar. Generally, the required equipment consisted of:

- Range camera SR4000
- White Spectralon target
- Dark grey Spectralon target
- 2 tripods
- 2 tripod stars
- Plane and even background
- Total Station *Leica* TCA2003

The characteristics of Spectralon targets as observation objects and the reasons for using them will be explained in the following sub-chapter 3.1.1.



Figure 7 – *Typical measurement setup*

Figure 7 illustrates the typical setup.

The camera and the target were placed on one tripod each. In addition, as all tests were realized indoors, the two tripods had to be put on tripod stars (as countermeasure for skidding). Camera and target were levelled and the target was centred in the camera's field of view.

3.1.1 Spectralon Targets

Pro-Lite's Spectralon targets were used for the data acquisition as observation objects. Pro-Lite claims that Spectralon "[...] is a solid thermoplastic that exhibits the highest diffuse reflectance of any material or coating in the 250-2500 nm band. [...] It is hydrophobic, thermally stable to 350°C, UV-resistant and chemically inert to all but the most powerful bases such as sodium amide and organo-sodium or lithium compounds. [...] Spectralon can be easily cleaned by washing." [16].

Due to its known reflectivity, the known (flat) surface geometry, the independence of environmental factors and because it is relatively easy to handle, Spectralon is a perfect material for observation targets.

Two different Spectralon targets of the company *Pro-Lite* were used: A white target with a reflectivity of 99% and a dark grey target with a reflectivity of 10%.

Figures 8 and 9 show a white and a dark grey Spectralon target during the experiments.



Figure 8 – *White Spectralon target*



Figure 9 – *Dark grey Spectralon target*

More information on Spectralon targets can be found on the *Pro-Lite* Homepage [16] and on the product sheet of the Spectralon targets (see A.2).

3.1.2 Software

The software used for data collection was the *Mesa Imaging Demo Software SwissRanger 3D Viewer Application*. This program was supplied with the range camera and can easily and intuitively be applied to gain data with the SR4000. The graphical interface immediately gives quick overviews of the data collected afterwards. The software generates three different output images. These are represented in the graphical interface and include:

- Distance Image:
In this image the measured distance values are displayed. With the checkbox 'Coord Transf' (which stands for coordinate transformation) it can be controlled if either the radial distances (box not checked) or the distances along the z-axis (= optical axis) of the camera are shown.

- Greyscale Image:

Here, the amplitude values are analysed. Depending whether the mode 'Convert Gray' is activated or not, the raw amplitude signals or converted values are displayed. This conversion is particularly important for the graphic representation of the amplitude data. As the illumination decreases with the square of the distance, amplitudes for more distant objects are much lower than the ones for nearer objects. To eliminate this effect the amplitude values are multiplied by a factor of the square of each distance. At 2.5 m distance (half of the feasible distance) the converted value corresponds to the original amplitude value. The result - a Greyscale Image with similar brightness of near and far objects - is visually similar to an image from a digital camera.

If the 'Convert Gray' mode is deactivated, the resulting image shows the simple amplitude values.

The amplitude values are 16 bit values, which corresponds to a range of 0-0x7FFF. Higher amplitudes correspond to higher values, the maximum value represents saturation.

- Confidence Map:

With the Confidence Map it is very easy to roughly estimate the quality of the data. The big advantage of this image is that in case of useless data this fact is obvious immediately, settings can be changed and new data can be gained straightaway. It is shown how certain the distance measurement of each pixel is. The confidence value for each pixel is calculated by a combination of amplitude and distance measurements and their variations.

Due to the immediately displayed quality of the data, regions of higher quality can be found and in case selected easily. It also supports the decision whether the chosen values for the parameters are appropriate or if these values have to be changed to achieve data of good quality.

The range for the confidence map is 0-0xFFFF, higher values mean higher quality.

The changeable settings in this software are the integration time on the one hand and the number of frames on the other hand. In addition, an amplitude threshold can be used but this fact was not considered in this thesis. "The integration time is the length of time that the pixels are allowed to collect light [...]" ([19], 35) The choice of the integration time is very important because too high integration time leads to saturation while too low integration time causes noise (more in 3.1.4). As indicated in 2.1.2 four samples

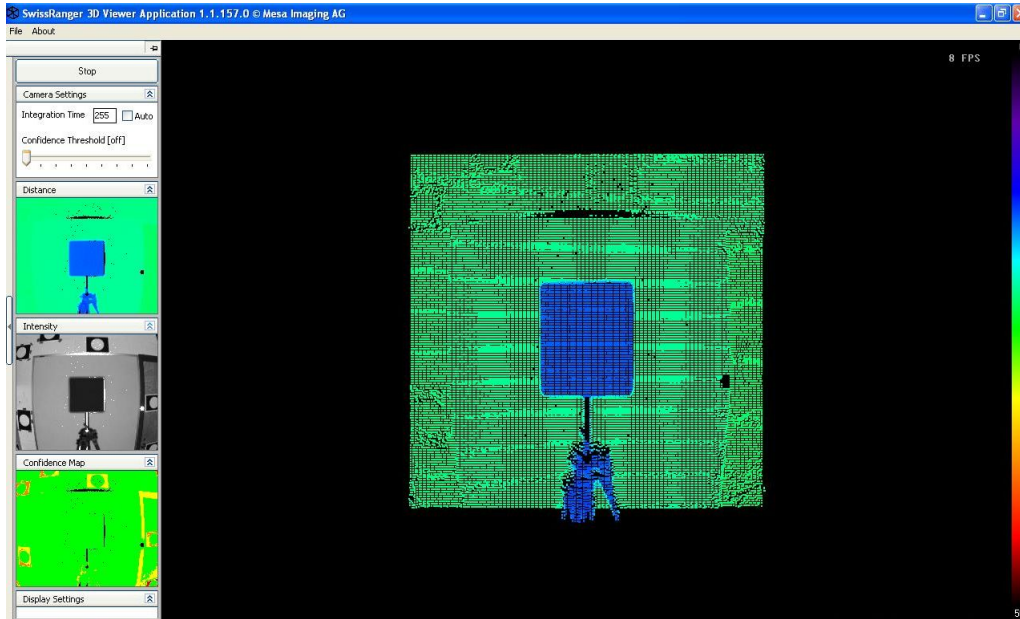


Figure 10 – *Mesa Imaging Demo Software SwissRanger 3D Viewer Application*

are needed to infer on the signal phase. Each sample needs one integration period. The time required to produce an image hence consists of four times the integration time plus four times the readout time. The possible integration times which can be chosen are 0–255 (steps of 1), which corresponds to 0.3–25.8 ms.

The number of frames indicates the number of repeating measurements with a specific frame rate. This frame rate is indirectly proportional to the integration time. Averaging over multiple frames can be useful to obtain higher accuracy.

For each frame a separate output file is generated. Each file contains coordinate and amplitude information in five arrays (one array has 144 rows and 176 columns, corresponding to the measurements of each single pixel). The first three arrays represent the Z, X and Y coordinates, the following array the raw amplitude values and the last array shows the values of the confidence map.

Figure 10 shows a screenshot of the Demo Software.

3.1.3 Reference Survey

To draw a comparison between the distance measurements of the camera and the actual distances between the SR4000 and the Spectralon target another measure had to be taken: The actual ranges must be determined precisely. Therefore, it was decided to use a total station *Leica* TCR803. The distances measured this way will be called 'Ref-Dist' in the following. Below, the measuring method will be described. Analysis and results follow in section 4.6.

The range camera and the Spectralon target were both attached to a tripod. The approach for the acquisition of reference data was as follows: The camera had to be replaced by the total station and the target had to be exchanged by a reflector.

This method required a consideration: When measuring distances with a total station and a reflector, the beam is deflected within both instruments. Thus, the distance measurements distort and obtain an offset. The resulting range thus can't be referred to the vertical axes of both instruments, which in turn are used for centering on the measuring points. Fortunately, these deviations are corrected automatically when measuring with a total station to a corresponding reflector; all distance measurements can be related to the vertical axes respectively to the measuring points situated below.

This differs from the measurements of a range camera to a Spectralon target: Offsets are not produced by beam deflections inside the instruments but by sending out and reflecting the beam not in the plane of each vertical axis. These offsets (one at the camera, one at the target) are not considered automatically and thus have to be determined manually from the outside.

Regarding the range camera, the position of the origin of the camera's distance measurements had to be clarified first. A definition could be found in the manual: "The coordinate system used here is "Right-Handed", with z-coordinate increasing along the optical axis away from the camera [...]. [...] The origin of the coordinate system (0, 0, 0) is at the intersection of the optical axis with the front face of the camera." ([19], 24) . The camera was then put on a camera mount to ensure that it was centered on the tripod. The camera mount itself was fixed on the tripod.

The following draft (figure 11) shows the bottom of the camera to illustrate the offset:

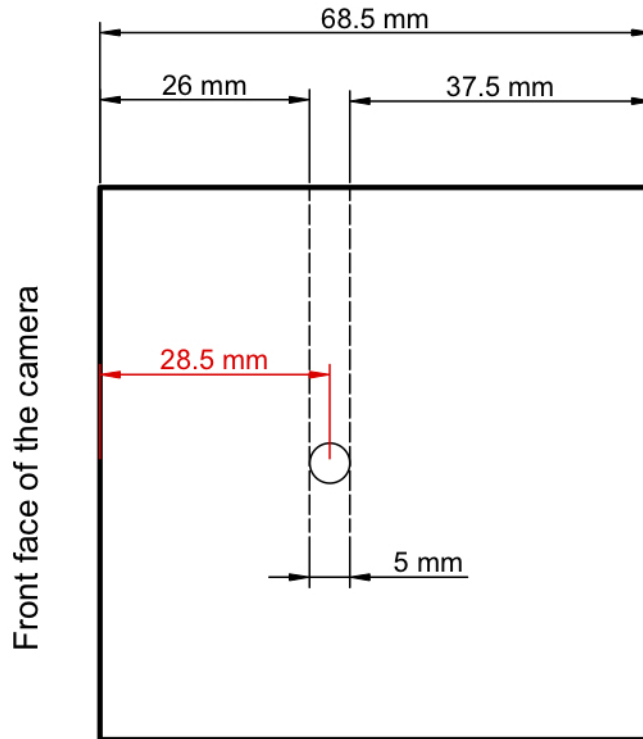


Figure 11 – *Calculated offset of the camera, layout of the camera's bottom.
The small circle represents the camera mount.*

To specify the offset of the camera, the distance between the front face and the center of the thread, where the camera is mounted on the camera mount (small circle in figure 11), had to be determined. Referring to figure 11, the black dimensions were measured with a *vernier caliper* (accuracy 0.5 mm). As a consequence, the interesting offset (red) could be calculated and specified to a value of 28.5 mm (The measured dimensions of the camera basically fit to the dimensions in the datasheet, see A.1).

Concerning the target, the strategy was more complex. Figure 12 shows the offset of the target in elevation (a) and groundplan (b):

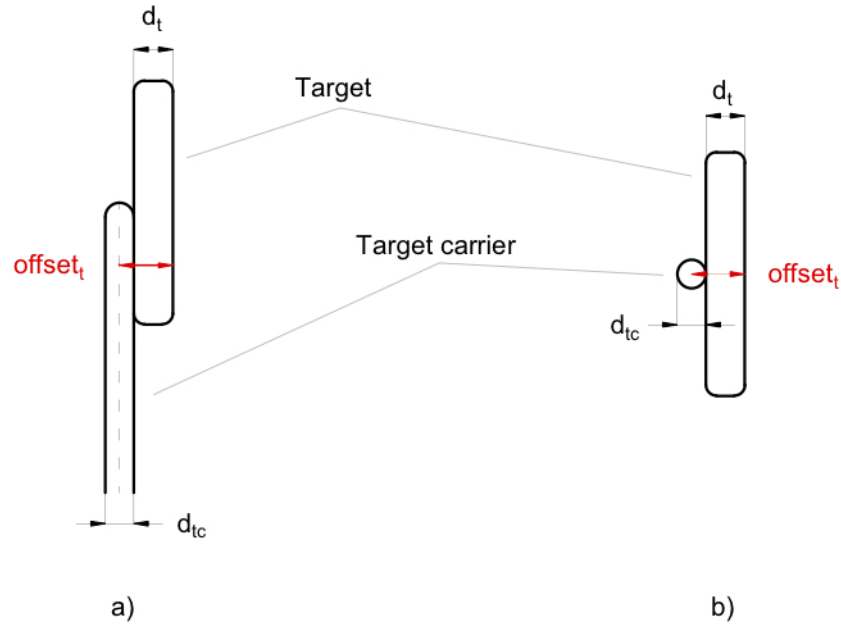


Figure 12 – Target and target carrier in a) elevation and b) groundplan

As can be seen in figure 12, the offset of the target consists of the diameter of the target itself (d_t) and the radius of the target carrier. d_t and the diameter of the target carrier (d_{tc}) were again measured with the *vernier caliper*, the final offset of the target (offset_t) resulted in:

$$\begin{aligned}
 \text{offset}_t &= d_t + \frac{d_{tc}}{2} \\
 &= 35 \text{ mm} + 11.25 \text{ mm} \\
 &= 46.25 \text{ mm}
 \end{aligned}
 \tag{9}$$

Now as the two part-offsets are set, the total offset can be determined. Both offsets effect that the measured distances of a range camera are shorter than the reference distances of a total station. Consequently, the sum of both offsets has to be subtracted from the total stations' distances to achieve comparability.

The final offset results in:

$$\begin{aligned}
\text{offset} &= 28.5\text{mm} + 46.25\text{mm} \\
&= \mathbf{74.75\text{ mm}}
\end{aligned}
\tag{10}$$

With these values being determined, the data of range camera and total station can be compared. Details and following analysis see section 4.6.

3.1.4 Operating the camera

Although each test certainly needs individual preparation, settings and performance for data acquisition, there are a few details which are identical for all four tests. These are described in this section.

As mentioned in 3.1.2, two variables have to be set before the start of any measurement: The integration time and the number of frames. As a compromise, the latter was given a value of 20 frames for all tests. With this chosen number of frames it was ensured that not too much data gets acquired but still enough to be used for calculating representative mean values. The integration time was adjusted for each test anew.

Regarding the integration time a different aspect had to be considered. Defining a proper integration time needs experiments in advance, regardless of which test is going to be implemented. As indicated in 3.1.2, the integration time defines how long the pixels are allowed to collect light. A higher integration time consequently signifies a larger quantity of received light. At a certain moment each pixel is saturated though. If light continues to be collected after this point of time, overexposure eventuates and the gained data is useless.

At the same time the integration time should be adjusted as high as possible as the noise minimizes with higher integration times.

In order to define this most suitable integration time, an experiment has to be carried out before each measuring, in which the highest integration time is identified without achieving overexposed data. In any case, this experiment has to be performed in the exact same setup as the following test itself. The final measuring arrangement thus has to be built up already before the specification of the integration time.

General requirements for all tests are constant environmental conditions. In addition, the camera must have been stored in the room of testing for at least one day as the measurements of a range camera also depend on changes

in the external temperature (e.g. [9]).

3.2 Warm Up Test

3.2.1 Task

At the beginning of a measurement process a range camera immediately starts to warm up after being connected to a computer even without acquiring any data. But independent of the camera's temperature, measurements are feasible anytime after the plug-in. To this effect several references (e.g. [4, 10]) indicate that a range camera needs a certain period of time to give a stable performance. This Warm Up test should hence help to find out more about the changes of the camera's performance with the increase of the sensor temperature. In addition, a timeframe for the necessary time to warm up should be specified.

3.2.2 Observation objects

As described in 3.1.1, two Spectralon targets are the main test objects of all experiments. The reason for using a dark grey and a white target is the completely different reflectivity of these two targets. Concerning the Warm Up test the reflectivity has no relevance though and therefore was studied in more detail in a different test (see 3.3). These facts led to the decision to use just one target here. The extent of the Warm Up test could be minimized this way, too.

The choice which target to use was based on integration time. The dark grey target experientially needs a much higher integration time for the same distance than the white one because dark grey absorbs a lot more light than white. It is theoretically possible to choose higher integration times than the indicated maximum integration time (see 3.1.2) but not in practice due to technical restrictions. As a consequence the white target was chosen.

3.2.3 Variables

The focus of this test was on time. To analyse only this single parameter, accordingly no other value was allowed to be changed during the measurement.

Before defining the important value of the integration time, the distance between the range camera and the target had to be specified. Decisive for the

choice of the distance in this case was the room setting though. At the beginning of the whole measuring process (the Warm Up test was the first test which was realized) no room at the institute was available that permitted the full choice of range. In the biggest available room the greatest possible distance from range camera to target amounted to roughly 1.6 m. As the distance was not part of the examined factors and hence not important for this test, the maximum distance of 1.6 m was chosen as final distance straight away.

In case of the Warm Up test an important factor had to be considered regarding the experiment of defining the best suitable integration time (see 3.1.4). Since the camera should be cool at the beginning of a data acquisition but warms up naturally while testing the integration time, this experiment had to be realized at least one day before the Warm Up test itself took place. This ensured that the SR4000 absolutely cooled down between these two start-ups and an entirely unaffected examination of the warm up time was possible.

With this consideration the used integration time was set to a value of 90 (which corresponds to a value of 9.3 ms) one day in advance.

Finally, considerations had to be given to the time interval in which the individual test data should be acquired. In preliminary tests an interval of five minutes was chosen. This time frame turned out to be too rough, the much smaller interval of 20 seconds was chosen in the end.

The following table 1 summarizes the chosen values of the Warm Up test:

Ref-Dist [m]	Integration Time [ms]
1.610	9.3

Table 1 – *Variables of the Warm Up test, white target*

3.2.4 Data acquisition and preprocessing

Before starting the observation, a general time frame had to be chosen. References [4] show, that the SR4000 needs about 40 minutes to be fully warmed up. But to be sure, a slightly extended investigation period was chosen in this project. With the settings described in table 1, data was captured each 20 seconds, 50 minutes all in all. The first measurements were taken right after the plug-in of the camera.

The acquisition of reference data with the total station (see 3.1.3) was performed before the Warm Up test as well. But the focus of this test was not on distances but rather on the time period in which the distance measurements turned stable. Therefore, precise reference distances are secondary. Thus a less complex (and less accurate) method for gathering reference data was chosen. By simply positioning a reflector on top of the camera (the center of the reflector right above the front face of the camera, definition of the origin of a range camera's measurements see Reference Survey, 3.1.3) and the target, horizontal distances and horizontal angles can be measured with the total station to the camera and the target. The horizontal distance from camera to target can hence be calculated with trigonometrical functions. For further analysis see section 4.6.

To get a first impression of the Warm Up test, a preprocessing was performed right after the data acquisition. A brief visualization should help to gain a first insight into the collected data. With the program *MATLAB* the data were easily imported and visualized. The preprocessing of the test (and in further consequence for the following three tests as well) concentrated mainly on two main observations: The range and the amplitude of the received signals. These two variables were displayed separately.

Regarding the Warm Up test, figure 13 shows the temporal change of the averaged measured distances during the Warm Up test.

As can be seen, a sharp increase occurs in the first 12 minutes. After this period of time the variations slowly level out until the distance measurements remain stable in a range of 2 mm after about 30 minutes.

Figure 14 shows the development of the amplitude of the returned signals. Although the decrease of the amplitude slows down after 11 minutes, it seems to never really tend to a value. Thus, the question arises to what extent the analysis of the raw amplitude is significant. In the preprocessing of the following tests (see 3.3.4, 3.4.4 and 3.5.4) just the range will therefore be analysed. The amplitude will be discussed in detail in chapter 4.

With the knowledge of the preprocessing, the temporary warm up time can be set to 30 minutes, which will be used in the following three tests. More details on the warm up time will be discussed in section 4.2.

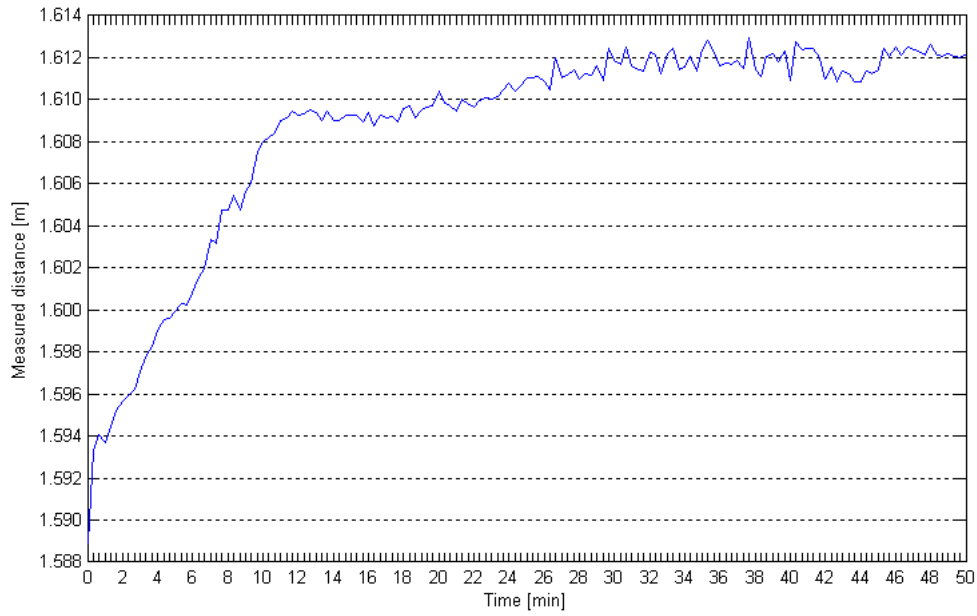


Figure 13 – *Temporal change of measured distances*

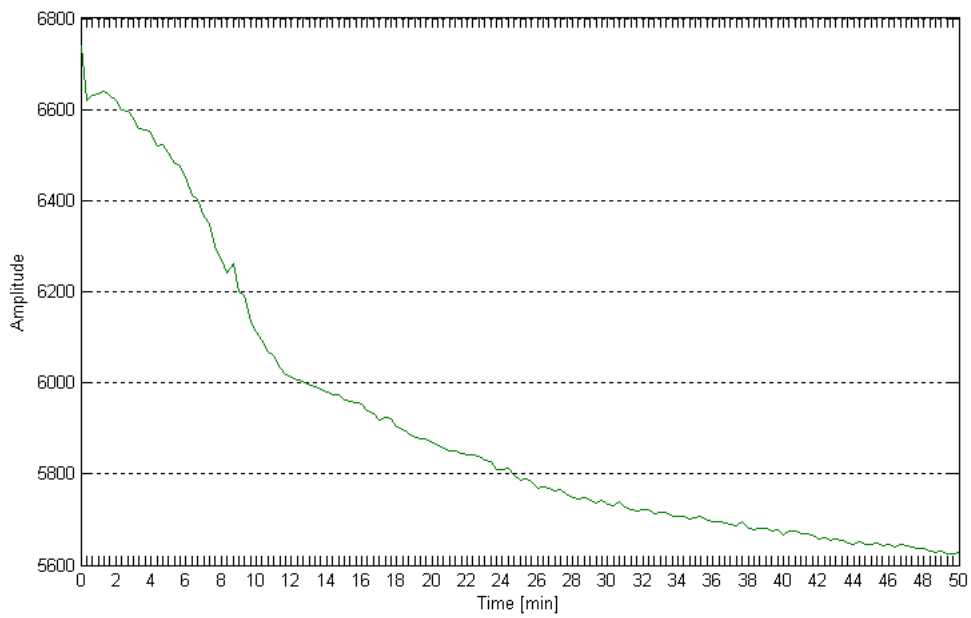


Figure 14 – *Temporal change of amplitudes*

3.3 Distance Test

3.3.1 Task

Generally, the SR4000 can be used for a range from 0.3 to 5.0 meters (see A.1). It is known though and can be read in different references (e.g. [4]) that the camera's results are dependent on the distance between camera and observation object. This problem represents the focus of this second test.

Hence, a closer look must be taken at the measurement accuracy. How does the accuracy correlate with the changing of the distance? While increasing the distance between camera and object, the reflected light power and consequently the measurement accuracy (with unchanged settings) decrease [20]. For analysing these issues the following Distance test was realized.

3.3.2 Observation objects

Unlike in the Warm Up test (see 3.2) reflectivity does play a more important role in the Distance test. In addition to the dependency between distance and measurement accuracy it is important to find out how the measurements are dependent on the reflectivity (3.1.1). As described before (see 3.3.1), the accuracy decreases with the increase of the distance when all settings stay unchanged. But what difference causes the influence of the reflectivity? How much does the accuracy differ between using barely and very well reflecting objects? To answer these questions it was decided to use both Spectralon targets, the dark grey and the white one. As described in the following chapter (see 3.3.3) more variables occur in this test, which makes the observation of the reflectivity even more valuable.

3.3.3 Variables

As the title of this test implies and was already mentioned before, the range represents the central value in the Distance test. Similar to the Warm Up test (3.2) just this single observed value should be allowed to change during the measurement process. The investigated distances between camera and target were defined in an experiment right before performing the Distance test itself.

According to the datasheet of the camera (see A.1) the shortest range with ensured entire functionality of the SR4000 is 0.3m. The shortest distance - which was set first - consequently must not be chosen lower than that. Following, the target's tripod and tripod star were placed and not moved anymore in the subsequent experiment and Distance test itself.

The tripod and star of the camera were then moved as close to the target's

tripod and star as possible (which came to a value of ~ 0.6 m). As this closest possible distance was longer than the required minimum distance, it hence defined the closest range for measuring. The first exact position for the camera's target could now be marked on the floor.

Starting from the closest distance, markings were then attached on the floor in intervals of 20 cm further and further away from the target. Although the official operating range extends just to a distance of 5 m (see A.1) the range was increased up to a value of ~ 5.4 m in order to study the behaviour of the camera beyond the nominal range.

After defining the measuring positions of the camera, the integration times had to be defined. As mentioned, the distance should be the only value changing in this test. Therefore, one integration time had to be chosen. Because this test was performed with both targets, an integration time for each target had to be chosen.

[9], [8] and [18] show that the range camera's results are also dependent on the integration time. To include this issue as well in the Distance test, more than one time for each target was chosen and the whole test was performed with each single integration time.

As described in 3.1.4, the highest possible integration time without achieving overexposed data had to be defined first for the closest distance and for both targets. Afterwards the most suitable integration times for the range of 5 m had to be found (the actual longest distance of this test of ~ 5.4 m was not used here because the camera was - as mentioned before - not expected to still produce proper results at ranges longer than 5.0 m).

Regarding the white target, the span between the integration times for the shortest and longest distance was quite big (values of 1.3 ms and 25.8 ms). Due to this fact three more integration times were chosen in between.

Concerning the dark grey target, the highest selectable integration time of 25.8 ms already was the best suitable integration time for a distance of only ~ 0.8 m. As a consequence, just two integration times were chosen for this target (12.8 ms and 25.8 ms).

Table 2 shows all distances and integration times for both targets.

3.3.4 Data acquisition and preprocessing

Referring to the first results of the Warm Up test the SR4000 needs about 30 minutes to be warm. This fact had to be considered before the execution

Ref-Dist [m]	Integration Times [ms]	
	Dark grey target	White target
0.599, 0.802, 1.002, 1.202, 1.197, 1.396, 1.599, 1.797, 1.996, 2.198, 2.397, 2.596, 2.796, 2.996, 3.197, 3.397, 3.598, 3.795, 3.999, 4.198, 4.398, 4.597, 4.798, 4.997, 5.197, 5.398	12.8, 25.8	1.3, 3.3, 8.3, 16.3, 25.8

Table 2 – *Variables of the Distance test*

of the data acquisition. Therefore, the range camera was plugged in before the setup of the Distance test or any experiments for preparation were performed. These arrangements took about an hour and guaranteed that the camera had completely warmed up when the actual test started.

After the warm up time had elapsed and the setup had been completed, the data acquisition started at the closest distance with one target and the corresponding values (see table 2). Once all integration times for this position and target were processed, the target was replaced by the second one. Again, data was captured with all integration times chosen in advance. After the first position had been completed, the distance between camera and target was increased by 20 cm and the just described acquisition process started again.

As already mentioned in 3.2.4, a preprocessing was performed after the collection of the data of this Distance test as well. Figure 15 shows the whole dataset.

It is salient that the higher the integration time the longer it takes to receive reliable data. This applies to both targets but becomes even more evident when looking at the graphs of the white target. This fact is likely caused by overexposure.

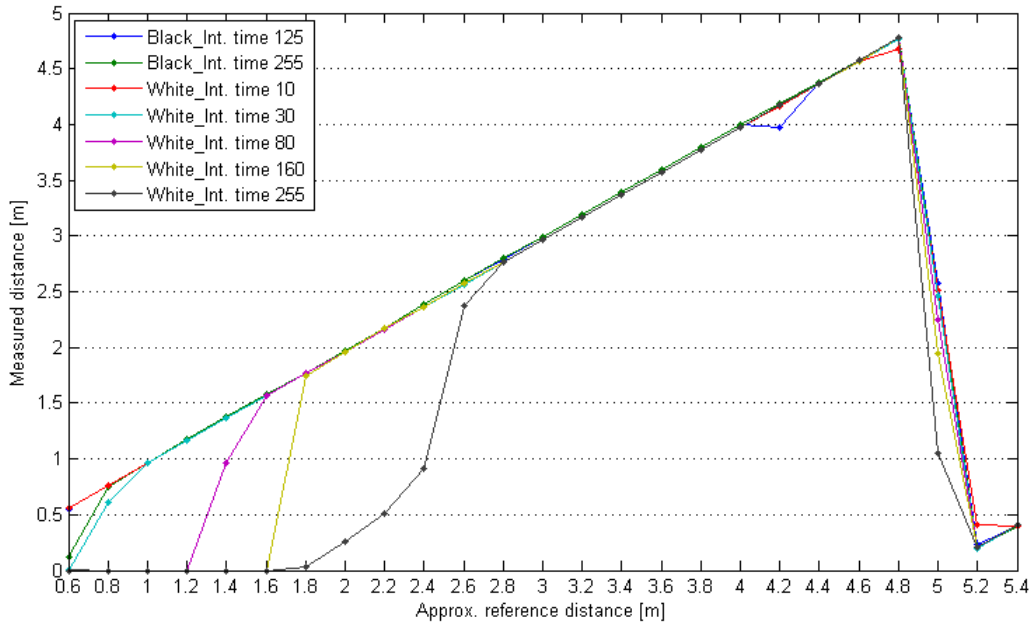


Figure 15 – Comparison between reference (*x*-axis) and measured (*y*-axis) distances

At the approximate distance of 5 m (exact distance: 4.997 m), the range camera did not yield reliable results anymore for any target and any integration time. This shows that the measurement range of 5 m should not be exhausted to the full limit. The question is now until which distance the SR4000 still delivers dependable results. But as no even more exact Distance test has been realised, it is just clear that a distance of ~ 4.8 m (exact distance in this test: 4.798 m) still ensures reliable results.

As figure 15 shows, all measured distances in the range of ~ 2.8 m - 4.6 m are quite similar. To get an overview of the actually occurring differences, the measurements at ~ 3.4 m are picked out (see figure 16).

Regarding figure 16, especially the two top lines (they represent the dark grey target) are conspicuous, which show a sharp distinction to the white target's graphs. This is true for the whole dataset. Differences in the distance measurement amount up to 3 cm between the white and the dark grey target. The reflectivity clearly affects the range measurements.

It is also visible that different integration times cause variations in the results. Variations between the measurements to one target make this obvious. These variations reach up to 5 mm. To follow this effect up, the next main

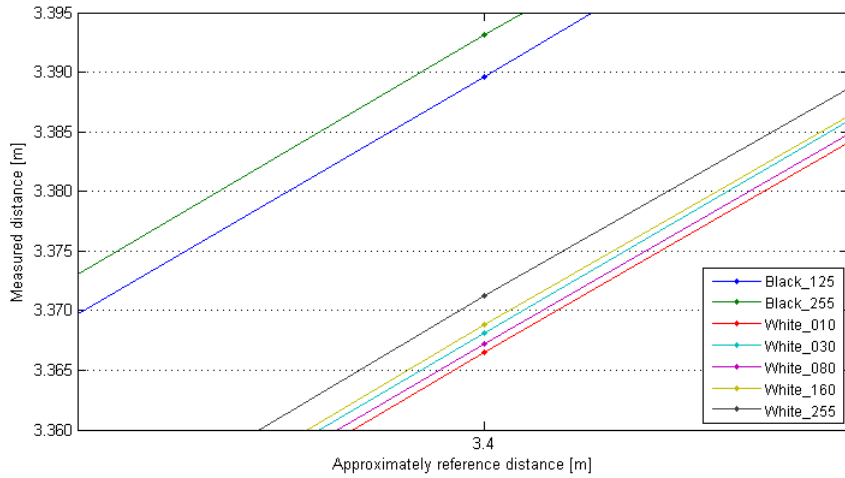


Figure 16 – Variations in range results at ~ 3.4 m

test dealt with the variable integration time (see 3.4). Further analysis of the Distance test can be found in 4.3.

3.4 Integration Time Test

3.4.1 Task

As mentioned above (see e.g. 3.2.3), the integration time determines how long each sensor pixel collects light. In the Distance test (see 3.3) it was shown that different integration times cause different results in the range measurements. To study this effect, the integration time has already been slightly varied in the last test (see Distance test, 3.3) but is going to be analysed in more detail in the following test.

3.4.2 Observation objects

To study the integration time, one target at one distance is, in principle, sufficient. Similar to the Distance test (see 3.3.2) the Integration Time test can give useful conclusions on the impact of reflectivity, too. In order to achieve that, again both Spectralon targets - dark grey and white - were used. By doing so it can be assumed that even more information on the correlations between results, accuracy and reflectivity can be gained.

3.4.3 Variables

Again the title of the test implies: The focal point of this test is on the integration time. All other variables consequently had to be set in advance to accomplish that this only value could be examined.

To determine the influence of the integration time as exactly as possible, the graduations of the integration time were chosen small. Starting with a minimal value of 0.4 ms and following value of 1.3 ms, the integration time was then increased by 1 ms each time (1 ms because of the equivalent to the actually entered integration time value of 10 - see 3.1.2). In this interval the integration time was enhanced up to a value of 25.3 ms. The highest possible time and concurrently last value to choose was 25.8 ms.

In the previous two tests the best suitable integration times without obtaining saturation had to be determined at the beginning. This step is not necessary for the actual test because the complete range of possible integration times is going to be applied anyway.

Apart from the integration time, the distance between range camera and target had to be defined, too. As mentioned in 3.3.3, the appropriate integration times for the dark grey and the white target on the same distance are relatively different. A dark grey target absorbs a lot more light than a white one and hence needs higher integration times on the same distances. Therefore, two different distances were chosen but both targets were used at both distances. Thus, suitable results for both targets could be achieved. The chosen distances were ~ 1.5 m and ~ 2.5 m.

The following table 3 shows the chosen variables for the Integration Time test:

Ref-Dist [m]	Integration Times [ms]
1.511, 2.503	0.4, 1.3, 2.3, ... , 24.3, 25.3, 25.8

Table 3 – *Variables of the Integration Time test, dark grey and white target*

3.4.4 Data acquisition and preprocessing

Referring to 3.2.4 and 3.3.4, again the warm up time of 30 minutes had to be considered before starting the actual test. But different to the Distance test the required time to set up the equipment was not simultaneously used to let

the camera warm up. As the setup for the Integration Time test was exactly the same as for the Distance test, the warm up time just had to elapse before the actual measurements could start.

As soon as this time had passed, the data acquisition started at the closer distance of ~ 1.5 m and with the dark grey target. The integration time was varied as described before (see 3.4.3 and table 3) from 0.13 ms right up to 25.8 ms. After this part of acquisition the target was replaced by the white one and the whole process started again. As a next step the distance between camera and target was increased to ~ 2.5 m and the acquisition process again was performed for both targets.

Following chapters 3.2.4 and 3.3.4 a preprocessing was accomplished after the data acquisition. Figures 17 and 18 show the data at distances of ~ 1.5 m respectively ~ 2.5 m, both with white and dark grey target.

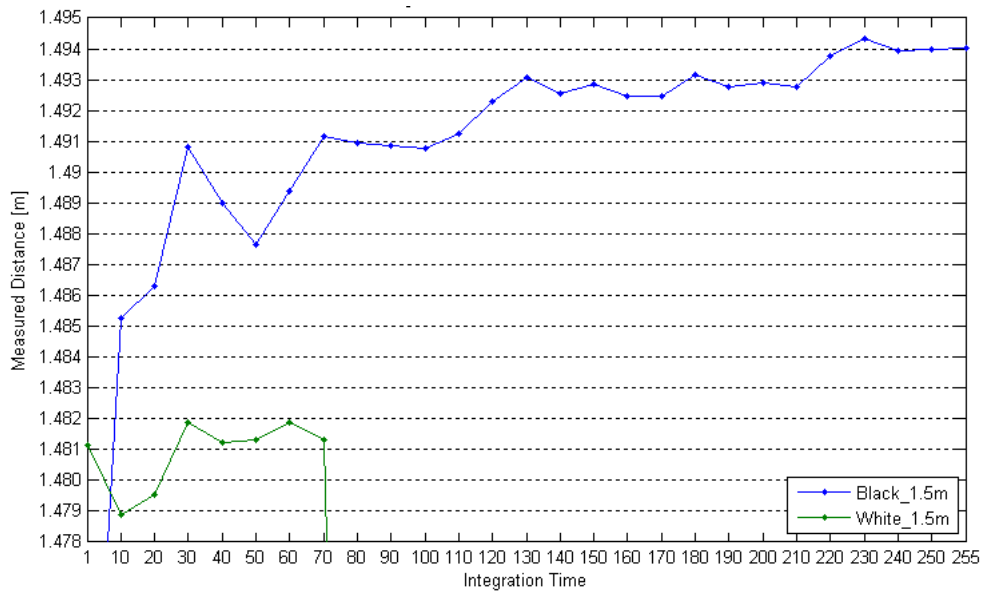


Figure 17 – Distance measurements depending on the integration time, ~ 1.5 m

It is obvious that at a distance of ~ 1.5 m and an integration time longer than 7.3 ms ($\hat{=}$ integration time of 70) overexposure eventuates with the white target. This is in line with the preprocessing of the Distance test, see figure 15. Up to this point there are differences in the measurements of up

to 1 cm between white and dark grey target.
 More can be seen at a distance of ~ 2.5 m:

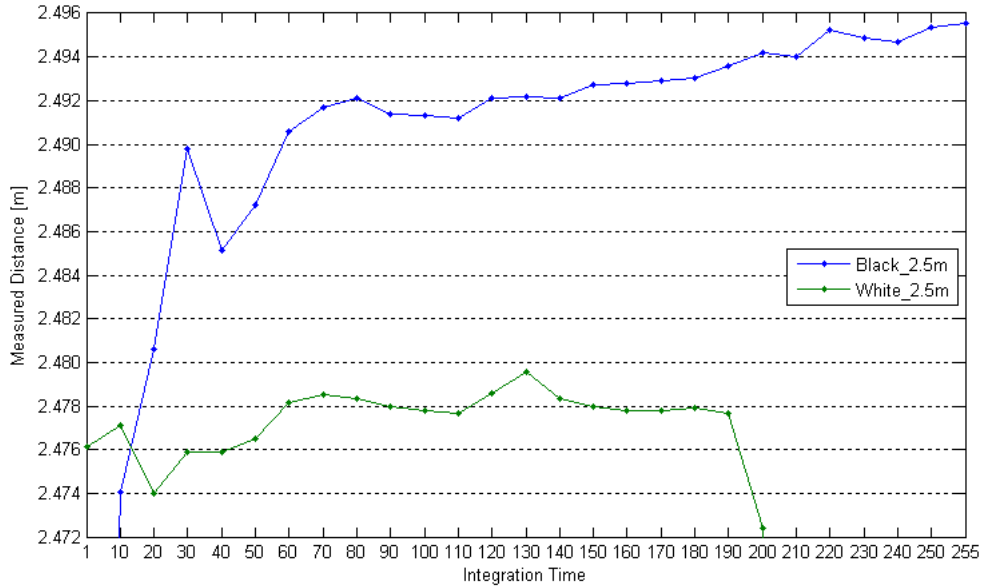


Figure 18 – Distance measurements depending on the integration time, ~ 2.5 m

Again, overexposure for the white target occurs; this time at an integration time of 20.3 ms ($\hat{=}$ integration time of 200). The differences in the distance measurements between white and dark grey target now rise up to 1.5 cm. While the measurements with the white target seem to tend to a value (~ 2.478 m), the data of the dark grey target increase steadily. This is similar to the behaviour in figure 17. More and detailed analysis will be addressed in chapter 4.4.

3.5 Background Light Test

3.5.1 Task

In chapter 2 it has already been mentioned repeatedly that light plays an essential role for range cameras. By a carrier wave which is sent out from a light source, the distance from camera to object can be determined. Also background light contributes to the achieved results although - as already indicated in section 2.3 - there are frequency band filters attached between lens and sensor to prevent background radiation from reaching the sensor. The SR4000 should not be used in sunlight [20] but even indoors some light

always permeates and affects the signal-to-noise ratio. To examine how extensive this effect is, is the goal of this Background Light test.

3.5.2 Observation objects

Again (see e.g. 3.3.2) it was expected that with this experiment also more insights into the influence of the reflectivity could be gained. In addition, the question arises whether there is as well a correlation between reflectivity and background light. So the decision was made again to use both, the dark grey and the white target as observation objects.

3.5.3 Variables

The key aspect of this test is the effect of the background light on the data. To examine this influencing factor, measurements should be done with background light in the observation room on the one hand and then with lights turned off on the other hand. To make a comparison between these different data sets possible, the settings (i.e. observation distance and integration time) must stay the same though.

The background light for the test was the ceiling lighting. In the room, two light bulbs each are placed in one lighting element, four elements are mounted in a row. Three of these lighting rows are integrated in the ceiling with a distance of about 1.5 m in between two rows. The lights are the *Philips F32T8/TL835*-Series with 32 watts. More information on the light can be found in [13].

First, the distance between camera and target had to be specified. As mentioned in 3.4.3, the results for the dark grey and the white target at the same distance and the same settings differ a lot. Hence two different distances were chosen to obtain suitable data for both targets. The final distances amounted - similar to the distances of the Integration Time test - to roughly 1.5 m and 2.5 m.

The preprocessing of the Integration Time test (see 3.4.4) showed that the gained data of the white target at a distance of ~ 1.5 m was overexposed starting from an integration time of 7.3 ms (see figure 17). This means that the span of suitable integration times is fairly small (considered a maximum value of 25.8 ms), which means less information as a consequence.

Concerning the dark grey target, the Distance test showed (see figure 18) that the highest possible integration time of 25.8 ms is already the best suitable time at a distance of only 0.8 m. Hence each distance was just used for

one target: The shorter distance (~ 1.5 m) for the dark grey target and the longer one (~ 2.5 m) for the white target.

Following 3.1.4, the highest possible integration times where no saturation eventuates had to be ascertained for each target at the corresponding distance. These best suitable integration times were 25.8 ms for the dark grey target (which is equal to the generally highest possible value) and 19.8 ms for the white target. For a greater amount of information two more times were additionally chosen for each target.

The following tables 4 and 5 give an overview of the chosen values for the Background Light test:

Ref-Dist [m]	Integration Times [ms]
1.501	15.3, 20.3, 25.8

Table 4 – *Variables of the Background Light test, dark grey target*

Ref-Dist [m]	Integration Times [ms]
2.512	10.3, 15.3, 19.8

Table 5 – *Variables of the Background Light test, white target*

3.5.4 Data acquisition and preprocessing

As already discussed in the last two tests (see e.g. 3.3.4), the camera needed ~ 30 minutes to warm up before the data acquisition could start. The setup for this last test was built up again in a different room (see Fig. 19) and the time for setting everything up was long enough to fulfill the required warm up time.

In the next step the experiment was started at the closer distance with the dark grey target. Data was gained with the described variables (see table 4), first with background light and then in darkness. Afterwards the range was extended to ~ 2.5 m and the process was repeated with the white target and appropriate settings.



Figure 19 – *Setup for the Background Light test*

For the Background Light test also, a preprocessing was performed. The following figures 20 and 21 show the acquired data of the dark grey target at a distance of ~ 1.5 m and the data of the white target at a distance of ~ 2.5 m.

Referring to figure 20, the occurring differences in distance measurements because of the background light amount up to 2–3 mm. Also, the integration time affects the measurements again. Differences of 2.5 mm are caused by it for the dark grey target.

For the white target (see figure 21) the background light causes differences of 1 mm while the integration time effects measurement differences of up to 4 mm. Compared to figure 20 it seems that the white target rather returns background light-independent data than the dark grey target.

This and more effects will be treated in chapter 4.5.

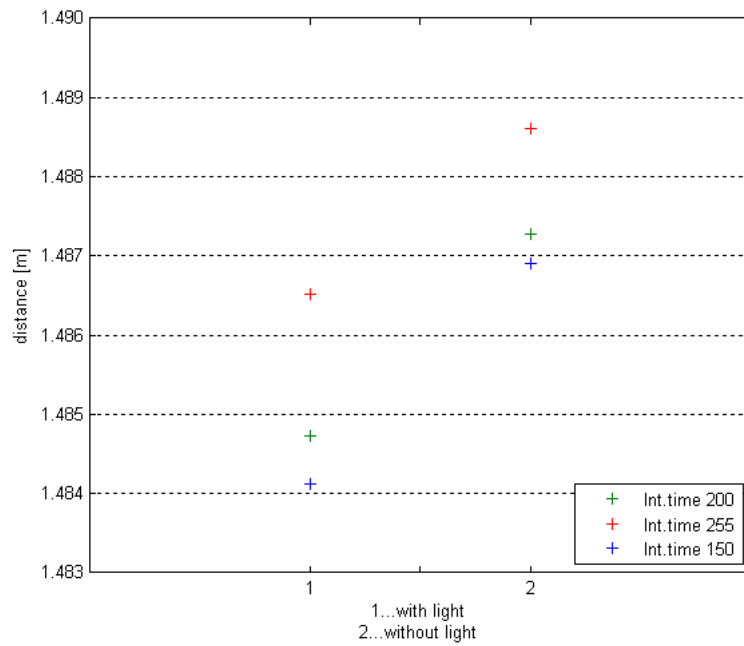


Figure 20 – Distance with (1) and without (2) background light, dark grey target

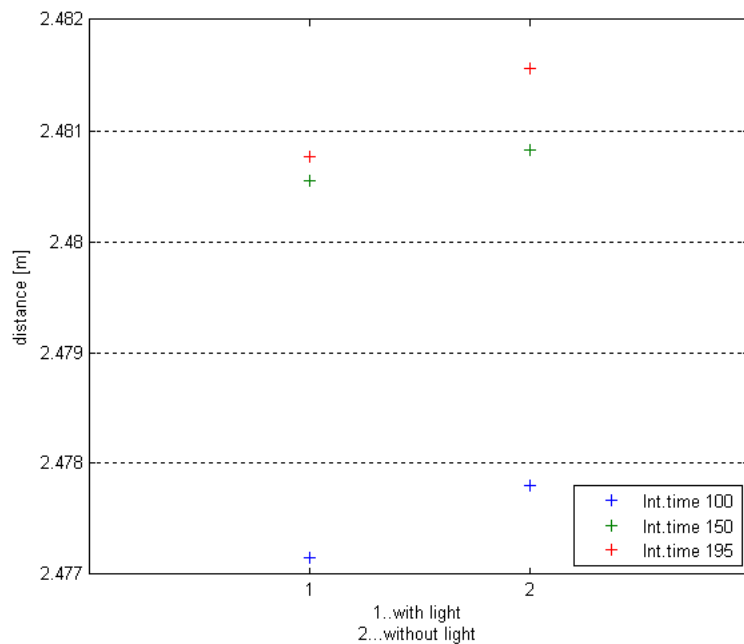


Figure 21 – Distance with (1) and without (2) background light, white target

4 Analysis

In the previous chapter 3 the realized tests were presented and the data acquisition was presented. In addition, a first visualisation of the data was performed. These steps gave a first insight into the four factors of influence which are examined in this thesis. Now in chapter 4 the data will be analysed. Initially, general preliminary processes will be introduced which are important for the whole amount of data. Then, structurally similar to chapter 3, each test will be described in detail and analysed thoroughly. Eventually, another focus is turned to the results of the reference survey introduced in 3.1.3.

All calculations and visualizations have been performed with the program *MATLAB*.

4.1 Preliminary Processing Measures

Before the analysis can be proceeded with, a rough adjustment of the whole amount of collected data has to be implemented. Among other things, corrupt measurements (which are mainly characterized by a range of 0) make such an adjustment necessary. The preprocessing in the previous chapter (see e.g. 3.2.4) was accomplished with the original data although the quality of the data was roughly examined in advance to prevent an impact on the results because of too many corrupt measurements. However, now the data has to be corrected more precisely before starting with the analysis.

As already presented in 3.1.1, each test was performed with the white and the dark grey Spectralon target, respectively (except the Warm Up test, where the white target was used only). Since the camera's field of view is larger than the extent of the investigated target in the field of view and just this area of the target is of relevance, the corresponding data was extracted from the total amount of data for each test.

The next step was an 'averaging'. This step helps to reduce the noise to such a level that the influence of random errors decreases. As mentioned in 3.1.4, with each measurement 20 frames were acquired. These frames hence are used to calculate representative mean values for this measurement. Thus, each representative pixel value is calculated as a mean value of the corresponding pixels of all frames. Here it certainly has to be considered that the data was captured in a continuous mode. As the manual explains, each first captured frame in the beginning of a measurement is acquired with the settings of the previous measurement: "In 'Continuous' Mode, because of the

1-frame latency, any changes in mode, integration time or modulation frequency setting do not affect the first acquired frame after the setting change, since this frame would have been acquired before the setting change.” ([19], 22). Hence, just the frames 2–20 were used for the averaging.

For the further tasks, the 'adjustment of independent observations', a representative variable for the distance is needed, which can be analysed in detail. As the object of interest in all tests is a target which represents a plane, fitting planes are calculated with the least squares method to model the targets in a first step. The distances between the fitted planes (from the middle pixel of the target, where x- and y-coordinates equal 0) and the origin of the camera's coordinate system (see section 3.1.3) represent an adequate measure for analysis. Other representative variables, for example the parameters of the fitted planes, are mentioned separately in the following sections where they are used. In figure 22 an example for a fitting plane with the corresponding distance data is presented.

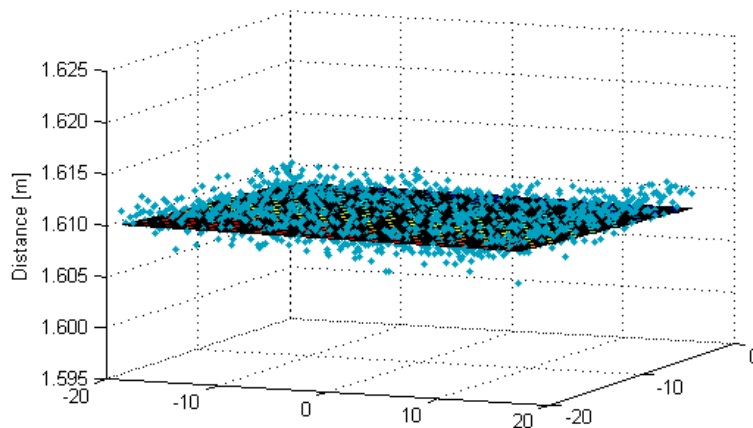


Figure 22 – *Example of a fitting plane*

Similar to the distance, a representative variable for the amplitude is required. The amplitudes are assumed to decrease symmetrically from the middle pixel in a non-linear fashion due to four different factors:

- Increasing distance
- Non-uniform illumination
- Vignetting
- Reflection behaviour of Lambertian surfaces

According to the manual [19] the first two factors are taken into account automatically. The two remaining factors are still reason enough to state that the spatial spread of the amplitudes is a paraboloid with the general form

$$A = a \cdot x^2 + b \cdot y^2 + c \cdot xy + d \cdot x + e \cdot y + f \quad (11)$$

where A represents the observed amplitude and x and y the pixel-coordinates in the image plane. The image plane and the object plane are parallel though, as a consequence the switching from image coordinates to object coordinates takes place.

Similar to the fitting planes the coefficients $a-f$ are determined by the least squares method for the modelling. Figure 23 illustrates an example of such a fitting paraboloid, plotted with the corresponding set of amplitudes.

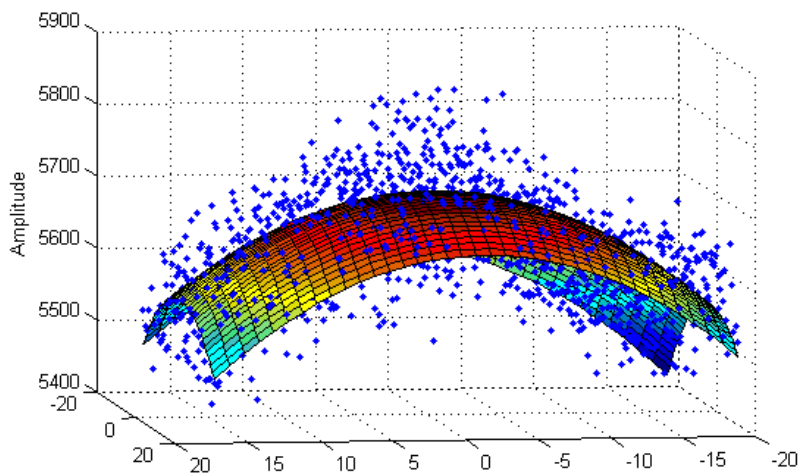


Figure 23 – *Example of a fitting paraboloid*

Figure 23 clearly shows the decrease of amplitudes from the middle pixel. In addition it can be seen that the data is not normally distributed around the center.

In the previously described steps of preliminary processing measures corrupt measurements are particularly important. Here, corrupt measurements are interpreted as outliers which are characterized by resulting ranges of 0. As the least squares method is not robust, randomly distributed measurement errors are indeed considered but outliers lead to a poor performance. Thus, outliers especially have to be taken into account.

Basically, there are two different types of occurring 0-values in the range. First, some pixels generate 0-measurements randomly and without an obvious reason as all pixels around yield consistent outcomes. This type of undesirable results is eliminated in the described process of 'averaging'. Second, there are pixels which permanently yield 0-measurements. These outcomes are removed during the mentioned plane-fitting.

As the preliminary measures are now carried out, the data is ready for analysis. In the following four sections the already presented tests (see chapter 3) will be analysed and described in detail. It is noted though, that some steps of the preliminary processing measures (e.g. the 'averaging') were also performed in the preprocessing.

4.2 Analysis of the Warm Up Test

The preprocessing of the Warm Up test in chapter 3.2 gave a first insight into the collected data of this first test and a provisional warm up time could be set to 30 minutes. Now, the aim of the analysis is to model the behaviour of the process of warming up.

Previous studies on the warm up time present some recommended time frames of warming up. Many tests have been accomplished with the SR3000, the predecessor model of the SR4000. Thereto, *Kahlmann et al.* [10] report a warm up time of 6 minutes to reach a range of distance variations of 5 cm. *Weyer et al.* [31] also recommend a minimum warm up time of 6 minutes while *Steiger et al.* [29] suggest a warm up period of 4 minutes minimum. The warm up time of the SR4000 on the other hand is an issue in [4]. Here, *Chiabrando et al.* recommend a time frame of 40 minutes for warming up but without specifying any range of distance variations at that point of time. The following subsections will present the results regarding the warm up time of this thesis.

4.2.1 Effects on distance measurements

As the data has been adjusted (see 4.1), the temporal process of the distances is examined at first. The result can then be compared with the results of the preprocessing (see 3.2.4). Figure 24 shows the outcome.

Basically, the behaviour of the graph in figure 24 is very similar to the comparable graph in the preprocessing (see figure 13). Nevertheless, in 3.2.4 it was

indicated that the distances sharply increase in the first 12 minutes. Compared with the preprocessing, this increase can be reduced to a time frame of approximately 10 minutes with figure 24. The difference of 2 minutes is explained by two factors. First, outliers were not taken into account in the preprocessing. Second, the fact that the number of range measurements with a value of 0 decreases with time. Hence, it can be stated that a longer warm up time leads to more reliable measurements in general.

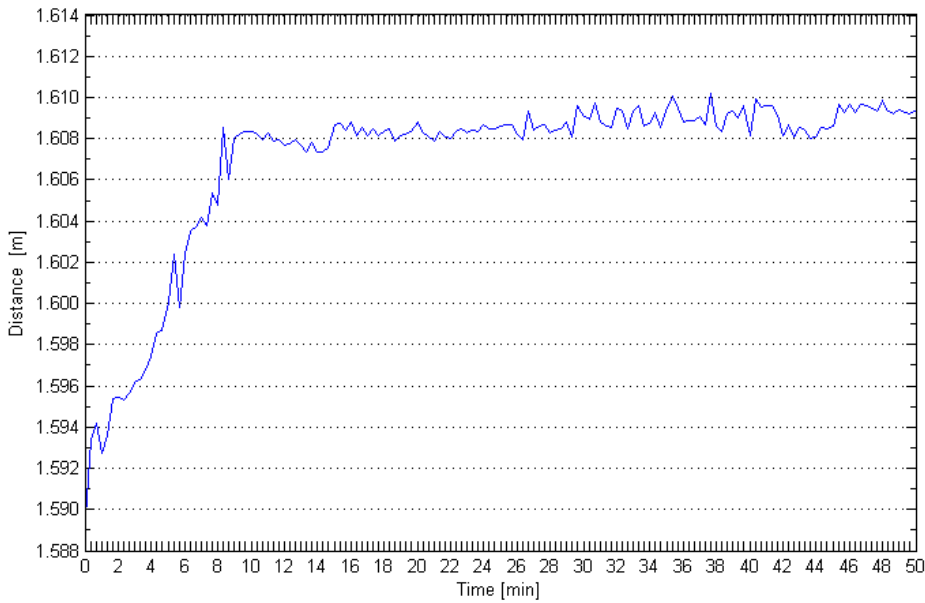


Figure 24 – *Temporal change of distances, based on the range between the origin of the camera’s coordinate system and the middle pixel of the fitting plane, respectively*

In addition, the trend in figure 13 tends to a distance of ~ 1.612 m. Here in figure 24, the graph converges to a range of ~ 1.609 m. This difference of 3 mm can be explained mainly by the different investigated variables. In the preprocessing, the mean values of the measured distances to all points of the target were plotted. Now, on the other hand, just the ranges to the middle pixel in the modelled plane are examined. Thus, the investigated distance decreases.

Based on figure 24, the process of warming up is modelled in a next step with an exponential function of the following structure:

$$y = a \cdot e^{bx} + c \cdot e^{dx} \quad (12)$$

where the coefficients a , b , c and d are determined by the least squares method. The decision which model to use was taken based on quality parameters such as SSE (Sum of Squared Errors of prediction) and RMSE (Root Mean Square Error).

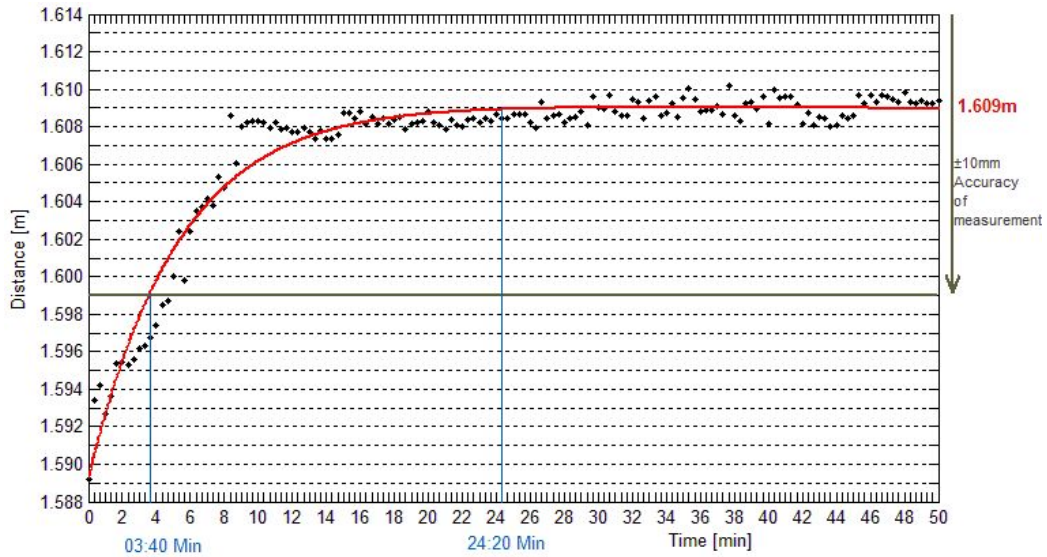


Figure 25 – *Modelled process of warming up*

Regarding figure 25, the red graph represents the previously presented modelling function. As can be seen, the model also converges to a distance value of 1.609 m. With reference to the datasheet of the SR4000 (see A.1), the range camera reaches an "absolute accuracy of ± 10 mm" (see A.1) at a given target reflectivity of 99% (which is the case in this test). This is interpreted as a tolerance and not in terms of a standard deviation. Based on a distance of 1.609 m, the measured data lie within this accuracy 5 minutes after the data acquirement has started. It is also visible that the graph stays constant after ~ 24 minutes and that the distance values vary in a tolerance of ± 1 mm after ~ 15 minutes.

4.2.2 Effects on amplitude measurements

After the adjustments in 4.1 also the temporal process of the amplitudes can be observed and compared with the corresponding figure of the preprocessing (see figure 14). Figure 26 shows the result:

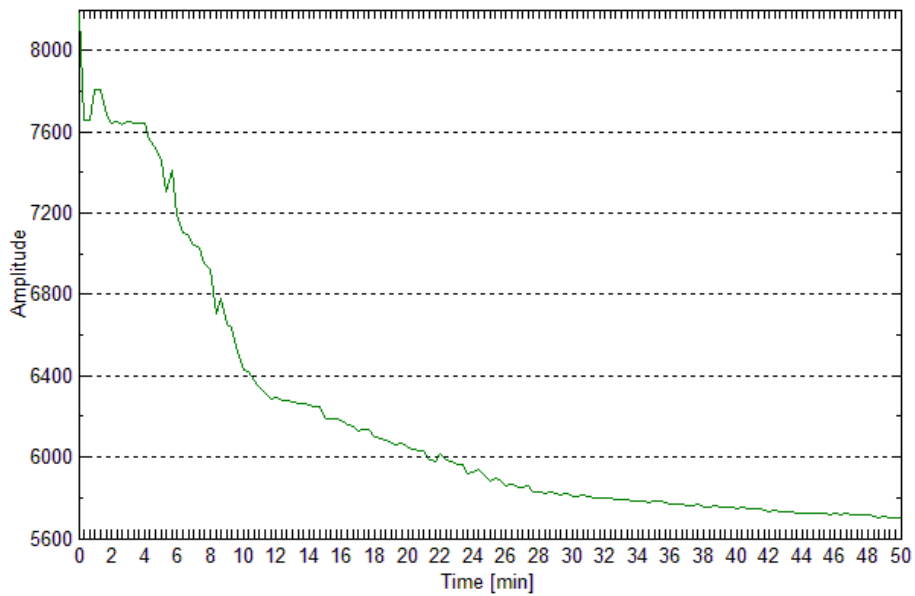


Figure 26 – *Temporal change of amplitudes, based on the least squares amplitude value of the middle pixel, repectively*

The general process of the graph in figure 26 shows many similarities to the comparable graph in figure 14. It is remarkable though, that the amplitude values are significantly higher in the first 15 minutes than in the preprocessing. This effect can be explained by the averaging which was performed in the preprocessing over the amplitude data of the whole target. In 3.2.4 it was mentioned that the graph does not seem to tend to a value. This statement is still applicable after the adjustment.

It is interesting to take a look at the adjusted parameters of the mentioned paraboloid (see 4.1). Figure 27 shows the adjusted parameters a , b , c , d , e and f .

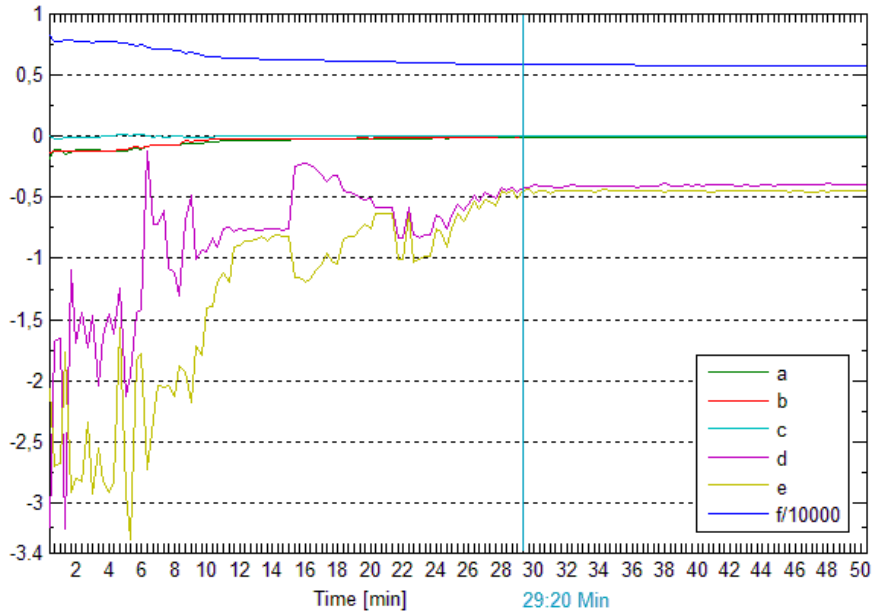


Figure 27 – *Trend of the adjusted parameters of the paraboloid*

Especially the parameters d and e vary noticeably in the first half-hour of the data acquisition. Also the parameter f mainly varies in the first 30 minutes, which is even more evident in figure 26. The graph in figure 26 represents the parameter f as it shows the amplitude values at the middle pixel (x- and y-coordinates equal 0).

The parameters $a-c$ get very low with increasing time but they never actually reach the value of 0. This means that these parameters still affect the image edges which further implies that the chosen model of a paraboloid is justified. After a warm up time of 50 minutes the parameters have the following values:

$$\begin{aligned} a &= -0.012 \\ b &= -0.006 \\ c &= -0.002 \end{aligned}$$

At the beginning of the data acquisition erratic changes occur. Only after 29 minutes the parameters $a-e$ stay stable. This is also confirmed by the standard deviation which is steady after the same time period of 29 minutes (see figure 28). The parameter f changes though until the end of the acquisition time, which implies that after 29 minutes differences of amplitudes are no longer influenced by the behaviour of the warming up. This leads to the conclusion that amplitudes as absolute measurements have to be used carefully, even after 50 minutes of data acquisition. Only differences of amplitudes can

be used without doubts after a warm up period of 29 minutes.

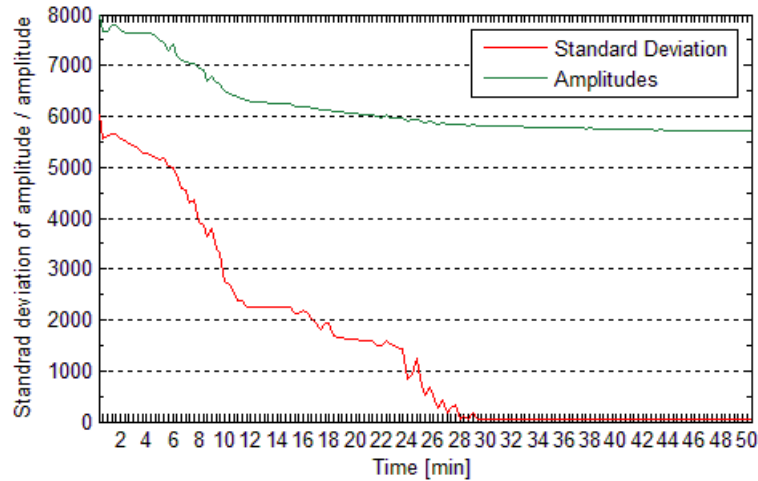


Figure 28 – *Standard deviation of the amplitudes*

The standard deviations of the amplitudes in figure 28 show that the amplitude values are not reliable before a warm up time of ~ 11 minutes. Not until then the standard deviations are clearly lower than the mean value. This is also confirmed by the coefficient of variation (CV) which shows a very similar plot as the standard deviation. The CV is very high in the beginning with a value of 0.74 and drops to a value of 0.36 after ~ 11 minutes. After 29 minutes the CV stays stable at a value of 0.009. The standard deviation reaches a value of 50 after 29 minutes and subsequently remains at that value.

4.3 Analysis of the Distance Test

Similar to the previous chapter 4.2, the results of the preprocessing in 3.3.4 will now be examined and consolidated in the analysis. In 3.3.4, the first insights into the data quickly showed differences in the distance measurements due to integration time and reflectivity. Differences of up to 3 cm could thus be made out. But errors in measurements are dependent on the distance, too. This issue will be the focus of the following analysis.

4.3.1 Effects on distance measurements

The number of measurements decreases with increasing distance. Hence, figure 29 at first gives an overview of the development:

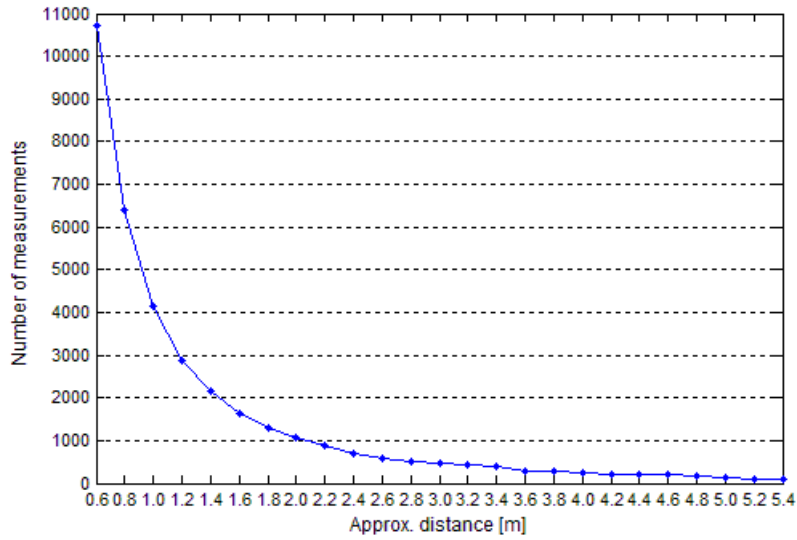


Figure 29 – *Number of measurements with increasing distance*

Especially the distances of ~ 1.5 m and ~ 2.5 m play an important role in the Integration Time test and in the Background Light test. The corresponding numbers of measurements of ~ 640 respectively ~ 340 are hence explicitly mentioned here.

Following 4.2.1, the main graph of the preprocessing is examined in a next step. Therefore, the 'averaging' of the frames 2-20 is processed and the fitting planes are calculated afterwards for each distance. This procedure was accomplished for each target and integration time. Based on the middle pixel for each fitting plane, the results are shown in figure 30. This output can be compared with figure 15 in chapter 3.3.4.

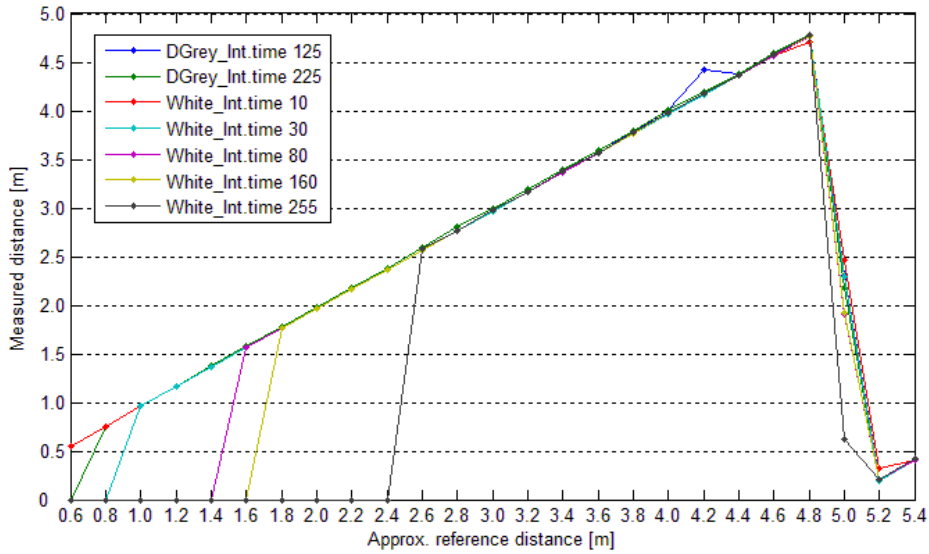


Figure 30 – Comparison between reference and measured distances, based on the adjusted data

Generally, figure 30 does not show a wide variance compared with the corresponding figure in the preprocessing. One difference is the process of the graph when overexposure occurs (this especially concerns the white target in the beginning of the data acquisition). While it looks more like an "incrementalism" to reliable data in the preprocessing, unreliable data due to overexposure is now clearly identified by values of 0 in figure 30.

The offset at an approximate distance of 4.2 m of the blue graph, which represents the dark grey target at an integration time of 125 ($\hat{=}$ 12.8 ms), is also noticeable. As compared to the preprocessing, the offset changed its tendency from a lower value to a remarkably higher value than the other curves depict at this distance. As no other graph shows a similar behaviour and the offset is not explicable by either overexposure nor an indeterminable distance, this offset is traced to a random error of measurement.

To get an impression of the measurement accuracy with increasing distance, the standard deviations of the distance measurements are examined in a next step. Two different modes of calculating the standard deviations are applied here:

- With mode A, the distance values of the middle pixel of each frame are used to calculate a mean distance and furthermore the standard deviation. Hence, no least squares adjustment is applied. As the ad-

justment is only based on the middle pixel, this method is referred to as the temporal distribution.

- Mode B represents the spatial distribution. Here, fitting planes are calculated for each single frame. For one measurement (i.e. frames 2–20 at one distance) 19 standard deviations a posteriori can hence be analysed.

First, mode A is applied. The outcome is shown in figure 31.

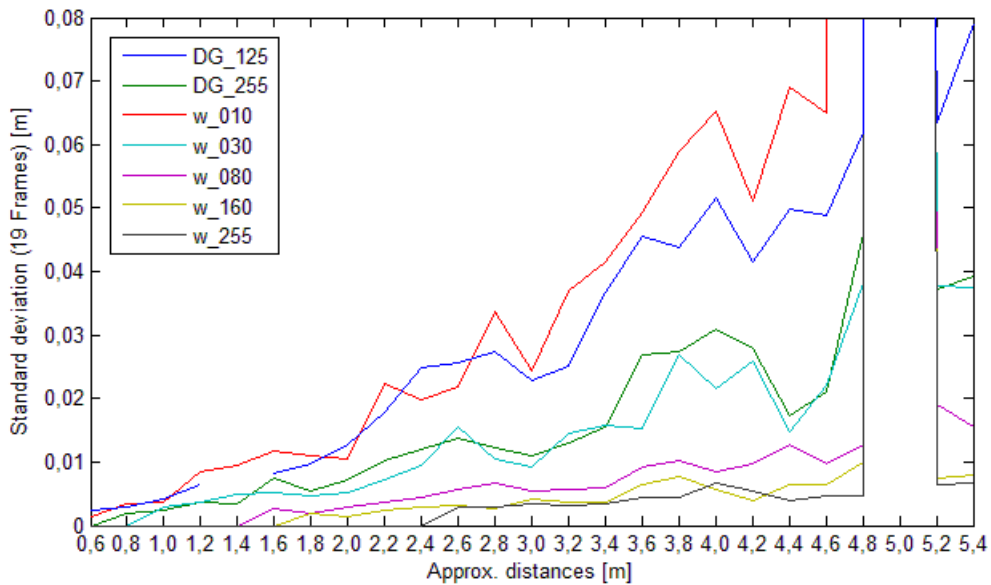


Figure 31 – *Standard deviations of 19 frames, based on the middle pixel*

When looking at figure 31 it is evident that the smaller the integration time, the faster the standard deviation increases. The highest measurement accuracy can thus be achieved by choosing the highest possible integration time. But this topic will be examined more closely in 4.4. Still, a closer look is being taken on the black graph, which represents the highest integration time of 255 ($\hat{=}$ 25.8 ms). Only at a distance of ~ 2.6 m, the range camera delivers reliable results as no overexposure eventuates. Until a distance of ~ 3.4 m the standard deviation is lower than 4 mm. From then on the standard deviation increases but stays lower than 7 mm until the distance of ~ 4.8 m.

The blue graph (representing the dark grey target at an integration time of 125 ($\hat{=}$ 12.8 ms) shows a gap at a distance of ~ 1.4 m. Here, no reliable data was available.

At ~ 5 m all standard deviations shoot up because the maximum working distance of the SR4000 is reached. The red graph (representing the white target

and an integration time of 10 ($\hat{=}$ 1.3ms)) shows this behaviour already at a distance of ~ 4.8 m. This corresponds with figure 30, where the red graph (same target and integration time) also shows a slightly different behaviour at a distance of ~ 4.8 m than all other graphs.

The dark green graph (dark grey target, integration time of 255) and the cyan graph (white target, integration time of 30 ($\hat{=}$ 3.3 ms) show a similar behaviour with partial overlaps. This effect is explained as the dark grey target has a 10% reflectivity, which is $\sim 1/10$ of the white target's reflectivity (99%) and the integration time for the dark grey target is ~ 10 times the integration time for the white target.

Interpreting the trend of the graphs in figure 31 it is stated that the standard deviation of distance is a function of the amplitude, as this determines how much energy is available for the measurement. The amount of energy is proportional to the reflectivity and the integration time while it is indirectly proportional to the square of the distance. Higher amplitudes furthermore lead to a better range accuracy. These statements yield the following equation:

$$\sigma_d = \text{function} \left(\frac{d^2}{R \cdot IT} \right) \quad (13)$$

with σ_d standard deviation of distance
 d distance
 R reflectivity
 IT integration time

To define the function, the following scatter plot illustrates the standard deviation of distances regarding the whole amount of data with the increasing term of $\frac{d^2}{R \cdot IT}$:

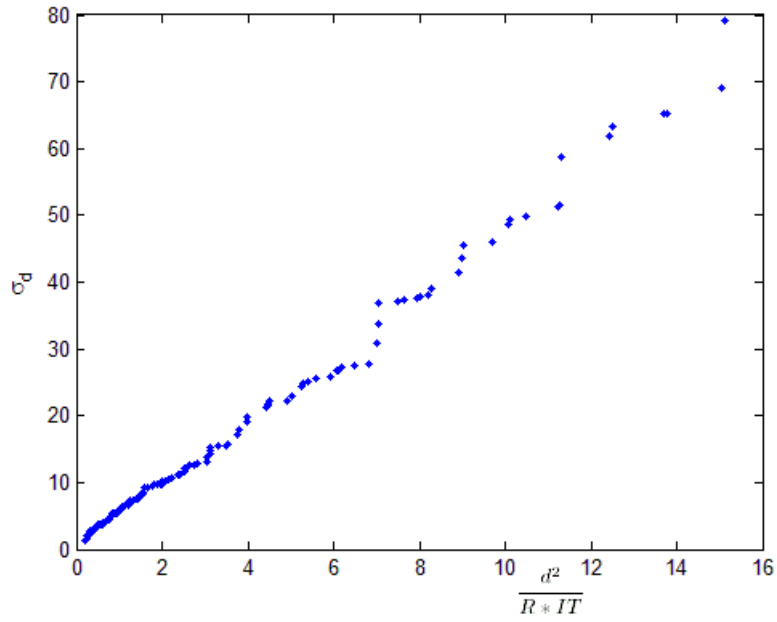


Figure 32 – Standard deviations of 19 frames, based on the middle pixel

Due to the clear result of figure 32, the required function is assumed to be linear. To determine the missing proportionality factor, the standard deviations are normalized according to equation 13 in the next step. Figures 33 and 34 show the normalized values for the dark grey and the white target. In the figures 35–37 the normalized values are categorized in three groups of distances. With figures 33–37 nearly the whole possible range of reflectivity (10%–99%) and distances (0.6–4.8 m) is covered.

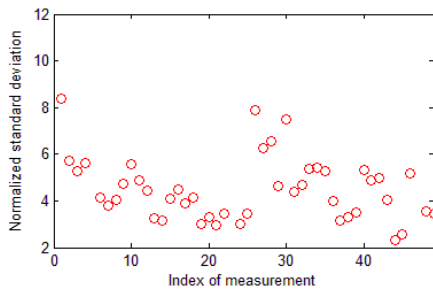


Figure 33 – Grey target

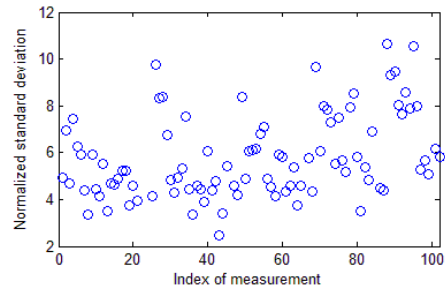


Figure 34 – White target

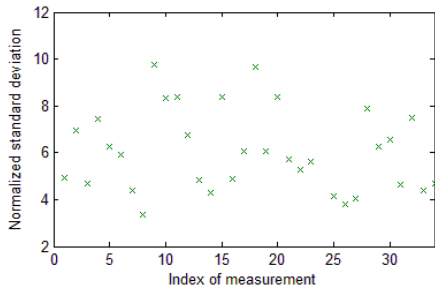


Figure 35 – *0.6–2.0 m*

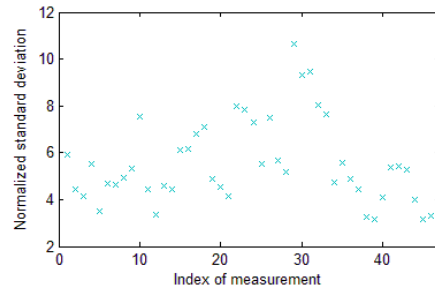


Figure 36 – *2.0–3.4 m*

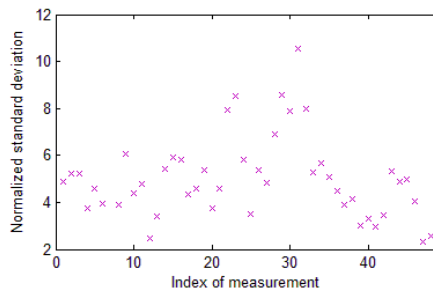


Figure 37 – *3.4–4.8 m*

The summarized normalized standard deviations (i.e. figures 33–34 respectively figures 35–37) can be displayed as a histogram, as the following figure 38 shows.

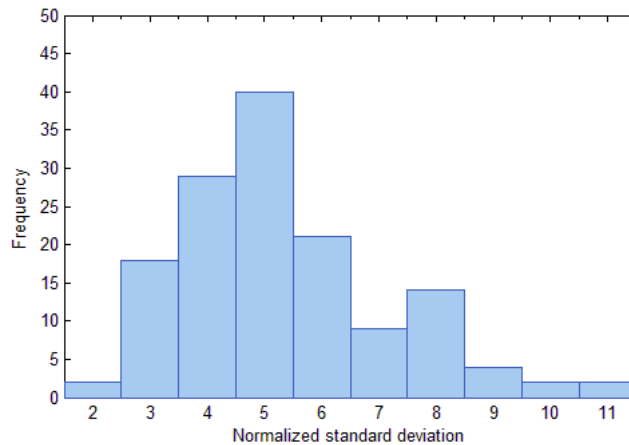


Figure 38 – *Frequency distribution of the normalized standard deviations*

As can be seen in figure 38, the largest number of normalized standard deviations ranges from 4.5 to 5.5. Hence, the proportionality factor is set to a

value of 5. Finally, formula 13 results for a standard deviation's dependency in:

$$\sigma_d[m] = \frac{5[100\frac{ms}{m}] \cdot d^2[m^2]}{R[] \cdot IT[ms]} \quad (14)$$

As a comparison to the just discussed standard deviations calculated with mode A, now the standard deviations per frame (mode B) are discussed. As each frame can be examined separately, this method would be of significance when the objects of interest are not static. Figure 39 shows the results:

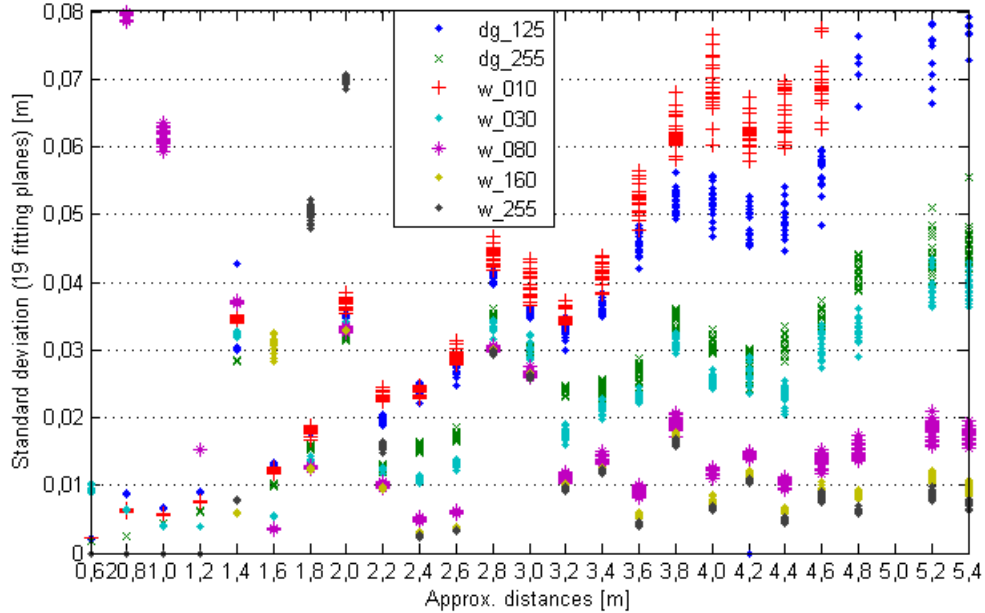


Figure 39 – *Standard deviations a posteriori for each frame, based on the middle pixel*

Compared with figure 31, the standard deviations in figure 39 are generally higher. This implies that the spatial distribution ($\hat{=}$ figure 39) shows a higher variance than the temporal one ($\hat{=}$ figure 31). In addition, random errors can be recognized in figure 39, especially at closer distances. As this fact is not applicable to figure 31, it can be said that the temporal distribution reduces random errors more effectively. For the time frame chosen for all tests in this study ($\hat{=}$ 20 frames) the temporal distribution hence is of greater significance than the spatial distribution. This fact can be explained by systematic errors,

which come into effect regarding expanse but not regarding time. In addition, random errors can also affect measurements, in so far as they get less accurate because they are closer to the edges of the field of view.

4.3.2 Effects on amplitude measurements

As not only the distance measurements are impaired by changing distances between range camera and target but also the amplitude measurements, these output values are examined in this section. Figure 40 illustrates the process of the amplitudes with increasing acquisition ranges, based on the middle pixel. The data of both targets and all integration times are plotted.

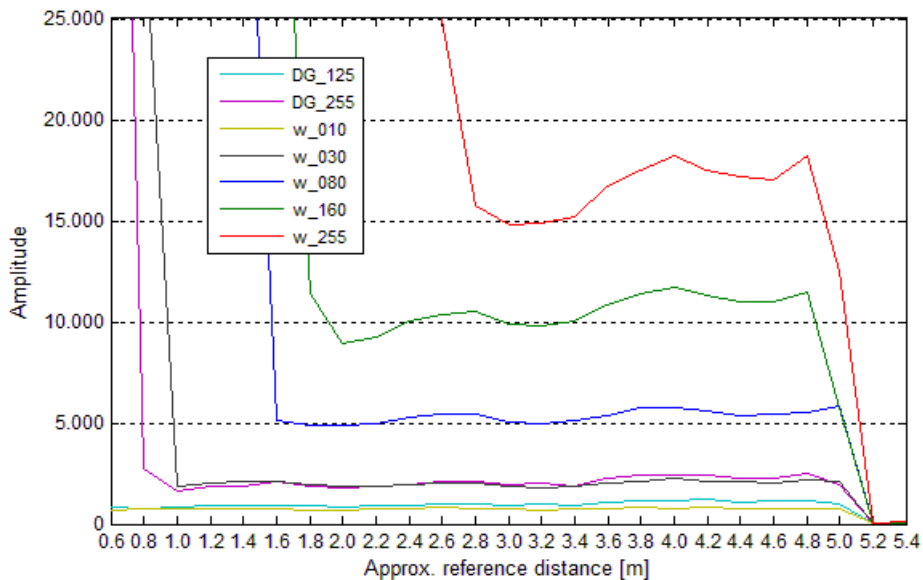


Figure 40 – *Amplitudes, based on the middle pixel*

At smaller distances often very high amplitude values can be noticed which drop to lower values at certain distances. Depending on the integration time and the object reflectivity, this drop happens at closer or further distances due to shorter or longer sustaining overexposure. *Frank et al.* [5] come to a similar conclusion examining another range camera.

Like the standard deviations of the distance measurements already showed (see figure 31), the similar behaviour of the dark grey target with an integration time of 255 ($\hat{=}$ 25.8 ms) and the white target with an integration time of 30 ($\hat{=}$ 3.3 ms) is noticeable. Due to the comparable proportions of integration times respectively the reflectivity, the two graphs show a very similar trend.

A quadratic decrease of the amplitudes with increasing distance was not expected as the distance as factor of influence is already taken into account (see section 4.1).

In a next step the amplitudes are normalized by division by the corresponding integration times and reflectivity (see figure 41):

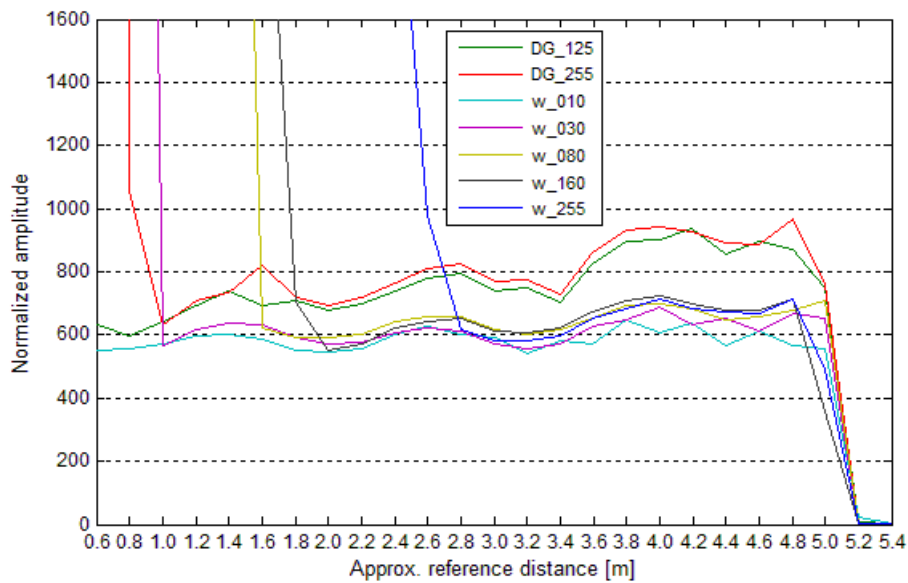


Figure 41 – *Normalized Amplitudes*

All graphs in figure 41 show a similar behaviour, which actually was expected. Also, the proportionality of the amplitude and the integration time respectively the amplitude and the reflectivity are recognizable.

4.4 Analysis of the Integration Time Test

In the previous chapter 4.3 it was already stated that the integration time impairs the accuracy of distance measurements (see equation 14). Also, the preprocessing of the Integration Time test (see 3.4) gave a first insight into the impacts of changes in the integration time on the measurement results. This effect will be examined in this section in more detail. In addition, the reflectivity as an important factor of influence was underlined in 3.4. This topic will also be discussed in this section.

4.4.1 Effects on distance measurements

First, the results of the preprocessing are examined with the adjusted data. Figures 42 and 43 show the process of the distance measurements with increasing integration time, based on the middle pixel of the fitted planes. These two figures can be directly compared with figures 17 and 18 in chapter 3.4.4.

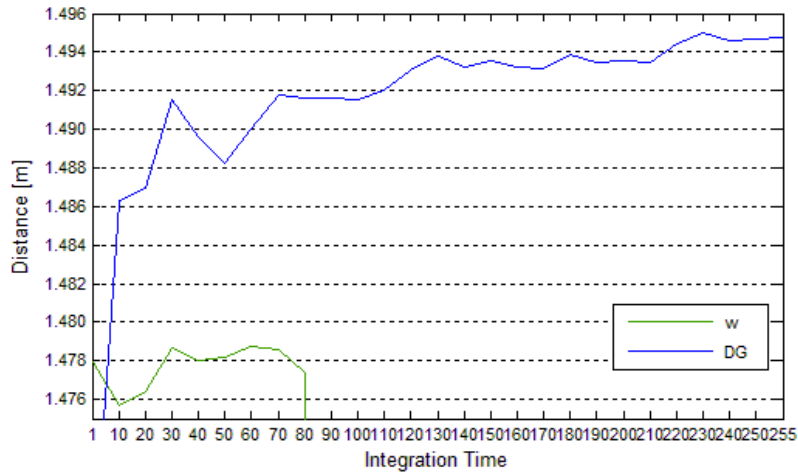


Figure 42 – Distance measurements depending on the integration time, based on the middle pixel, ~ 1.5 m

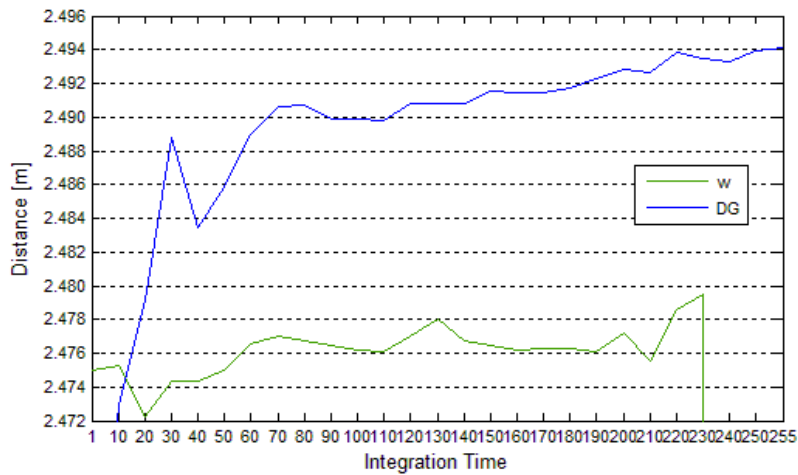


Figure 43 – Distance measurements depending on the integration time, based on the middle pixel, ~ 2.5 m

Compared to figures 17 and 18, the measurement differences between the

white and the dark grey target stay unchanged after the adjustment and still range from 1 cm to 1.5 cm, regarding both, the short and the long distance. As to the white target it may be noted that there are more reliable measurements in figures 42 and 43 compared to figures 17 and 18 before overexposure eventuates. Integration times of 80 ($\hat{=}$ 8.3 ms) respectively 230 ($\hat{=}$ 23.3 ms) can now still be used to achieve distance measurements (in comparison to 70 ($\hat{=}$ 7.3 ms) and 190 ($\hat{=}$ 19.3 ms) in the preprocessing). This can be attributed to the least squares adjustment and the integrated process of filtering 0-measurements (see 4.1).

Another similarity between figures 17–18 and figures 42–43 is the increasing drift of the distance measurements with the dark grey target. At both distances the corresponding graphs do not seem to tend to a distance value. The measurements with the white target, on the other hand, are stable in a range of 3 mm respectively 6 mm, regarding the short respectively the long distance. There is a slight jump just before the moment of overexposure in figure 43, though, which can hardly be explained as there is no similar behaviour in figure 42.

To take a look at the standard deviations of the distance measurements after the least squares adjustment, the standard deviations a posteriori are plotted in figure 44.

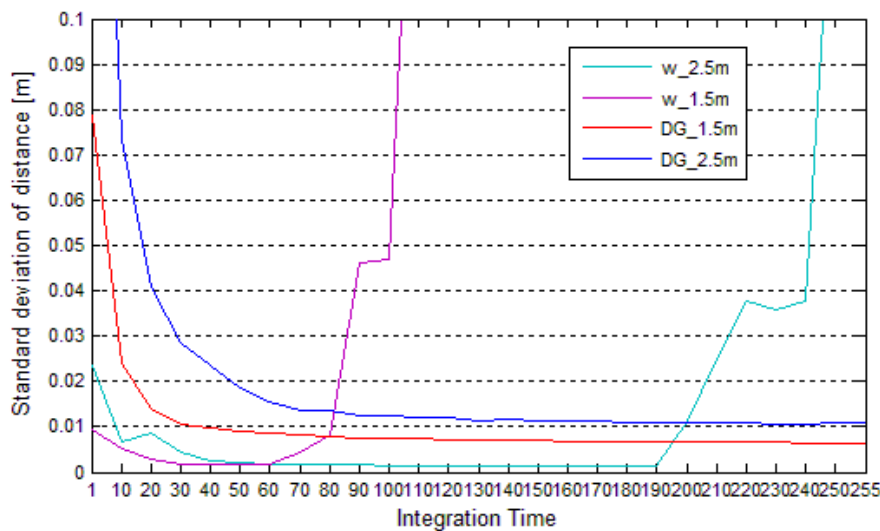


Figure 44 – *Standard deviations of the distance measurements a posteriori*

Figure 44 shows how important it is to define a proper integration time. Too low integration times lead to high standard deviations due to noise, which is

visible in all graphs. Too high integration times, on the other hand, easily cause overexposure, which happens with the white target at both distances. According to the standard deviation, integration times of 100 ($\hat{=} 10.3$ ms) respectively 240 ($\hat{=} 24.3$ ms) can still be used to gain reliable distance measurements with the white target. The standard deviations are actually a little bit higher here, but still reasonable. This increase of possible integration times compared with the distance measurements can be explained as the standard deviation concerns the whole target data while the distance measurements in figures 42 and 43 only represent the middle pixel. Regarding equation 13, figure 44 confirms that the standard deviation of the distance is inversely proportional to the reflectivity as the deviations of the dark grey target are significantly higher than the values of the white target. Furthermore, the inversely proportional influence of the integration time is also visible.

In general, it can be stated that an increasing amount of energy means higher measurement accuracy. At certain integration times, though, the standard deviations of the distance measurements get stable. This is recognizable in all four graphs in figure 44 and shows that the systematic errors start to dominate the result of the least squares adjustment. The increase of the integration time after these certain points does not lead to any further improvement in the measurement accuracy.

Similar to section 4.3, the normalized standard deviations are calculated following equation 13. The summarized deviations of the whole data set is plotted in the following histogram:

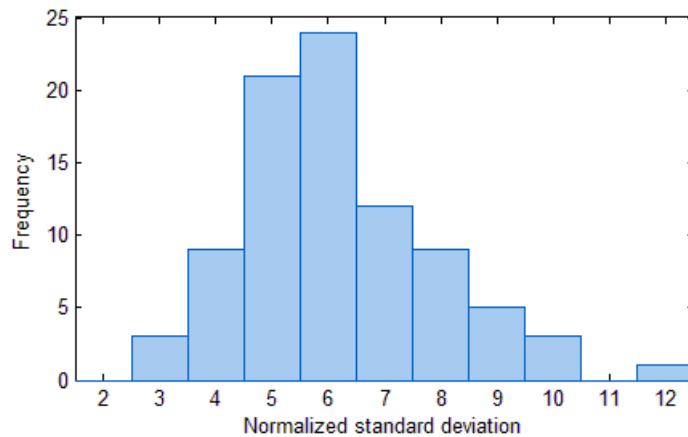


Figure 45 – *Frequency distribution of the normalized standard deviations*

Regarding figure 45, the mode of the normalized standard deviations is 6

(compared with a value of 5 in the Distance test (see 4.3.1). However, there is just a minor difference in the amount of values in the range of 4.5–5.5 respectively 5.5–6.5. The result is hence very similar to the statements made in section 4.3.1 and in equation 14.

4.4.2 Effects on amplitude measurements

After the least squares adjustment of the amplitude measurements (see section 4.1), the amplitudes - based on the middle pixel - and the standard deviation of amplitudes a posteriori can be examined. Figures 46 and 47 illustrate the change of amplitude values and standard deviations with increasing integration time for the dark grey respectively the white target. In both figures the two distances of ~ 1.5 m and ~ 2.5 m are shown.

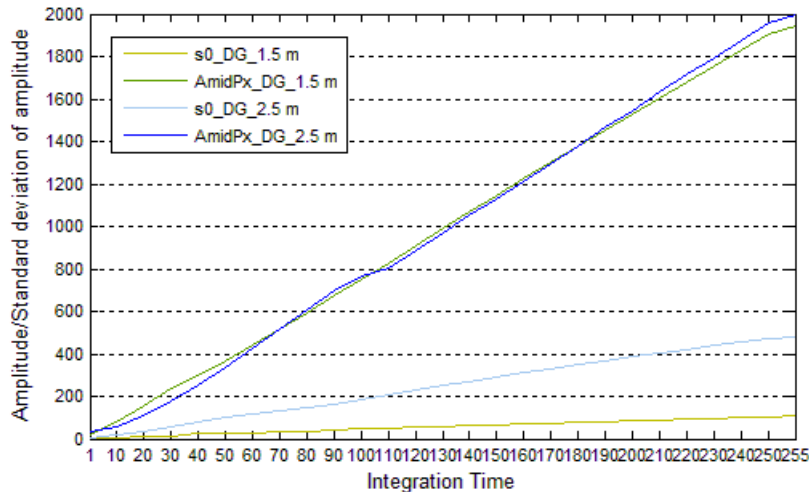


Figure 46 – *Amplitudes - based on the middle pixel - and standard deviation of amplitudes a posteriori, dark grey target*

The linearity between integration time and amplitude respectively integration time and standard deviation of amplitude is easily recognizable. In figure 47, which represents the white target, the linearity changes for both distances at certain integration times due to saturation. Due to this saturation the data is limited up to the integration times of 80 ($\hat{=}$ 8.3 ms) and 230 ($\hat{=}$ 23.3 ms), concerning the short respectively the long distance. Also the proportionality between the standard deviation of amplitude and the amplitude itself is noticeable.

At a distance of ~ 1.5 m the image section is larger than at a distance of ~ 2.5 m, hence more measurements are available. Especially figure 46 shows

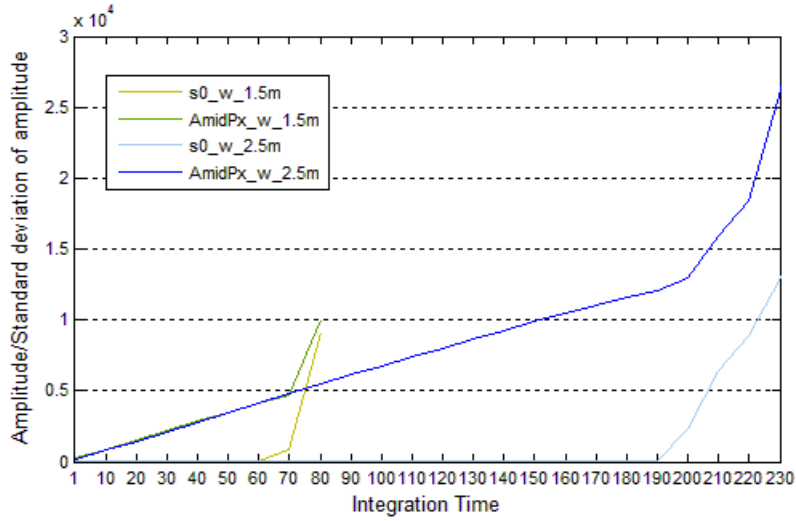


Figure 47 – Amplitudes - based on the middle pixel - and standard deviation of amplitudes a posteriori, white target

an important associated fact, namely that more measurements lead to a lower standard deviation of amplitude.

Figure 46 illustrates once more the difficulties with poorly reflective materials. Compared with figure 47, the dark grey target causes higher standard deviations especially at the longer distance of ~ 2.5 m due to its low reflectance. The standard deviations in figure 47, on the other hand, are very low for both distances before saturation eventuates as the white target is highly reflective.

4.5 Analysis of the Background Light Test

As already mentioned in section 2.3, the SR4000 has an integrated optical filter between lens and sensor which keeps background radiation from reaching the sensor. Some light nevertheless permeates the sensor and impairs the measurements. Section 3.5.4 already gave an insight into the effects caused by the background light, the following section will enlarge upon it.

4.5.1 Effects on distance measurements

Similar to e.g. 4.4.1, the first step of the analysis is to examine the graphs of the preprocessing with the adjusted data. Figures 48 and 49 illustrate the distance values after the least squares adjustment with and without background light for the dark grey and the white target, respectively. The observation distances came to ~ 1.5 m for the dark grey target and ~ 2.5 m for the white

target. The use of different distances guaranteed that no overexposure occurred for both targets (see 3.5.3). Also, three different integration times were used for each target.

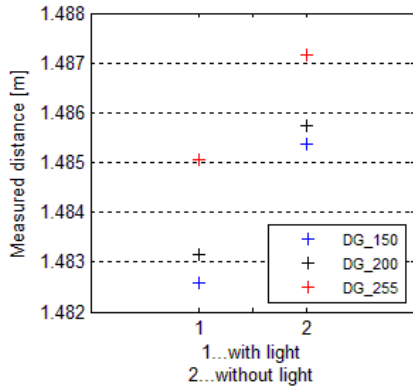


Figure 48 – Distances, dark grey target

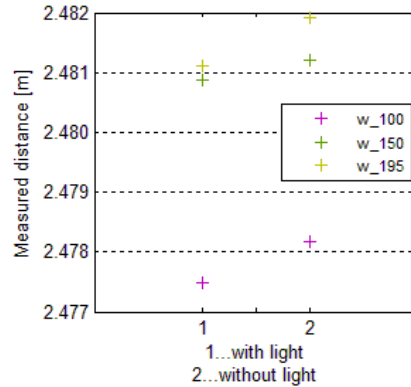


Figure 49 – Distances, white target

Previous analyses often showed lower distance values after the least squares adjustment due to the different examined values in the preprocessing respectively in the analysis (see e.g. 4.4.1). Compared with figures 20 and 21 in section 3.5.4, this is the case here, too. It is especially noticeable in figure 48, though, as the observation distance with the dark grey target is smaller than the distance with the white target.

As already pointed out in the preprocessing (see 3.5.4), the background light causes differences in the distance measurements of up to 2.5 mm with the dark grey target. The differences due to background light with the white target amount to less than 1 mm. This leads to the assertion that measurements with highly reflective objects are more robust against the influence of background light than less reflective objects.

Different integration times also cause differences in the distance measurements. This effect is reflected especially in the measurements with the white target as the differences amount to ~ 4 mm. This fact is not pursued at this point, though, as the amount of data is very small and the integration time as factor of influence has already been examined in more detail in 4.4.

The standard deviations a posteriori vary in a range of 0.5 mm with the dark grey target (see figure 50). With the white target the variations are even smaller (see figure 51). Hence, it can be stated that background light causes a constant systematic error in the distance measurements. The accuracy of

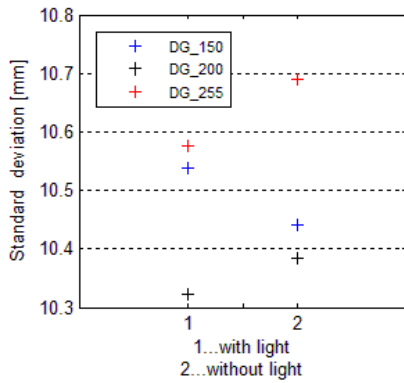


Figure 50 – *Standard deviations, dark grey target*

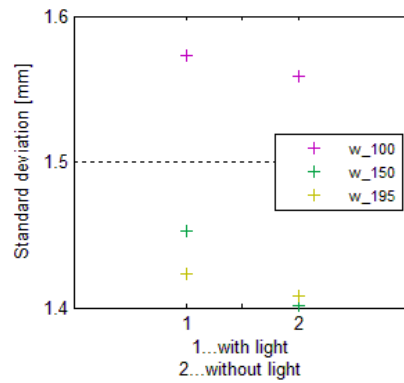


Figure 51 – *Standard deviations, white target*

the measurements just changes within a range of a tenth of a millimetre. These variations can hence be declared as irrelevant. Similar insights could be found in [25]. *Pattinson* tested a different range camera and declares that background light does not have significant effects on distance measurements and their standard deviations.

4.5.2 Effects on amplitude measurements

Also the amplitude measurements show that the background light only has little impact on the results. Figures 52 and 53 show the amplitudes a posteriori for the dark grey, respectively the white target.

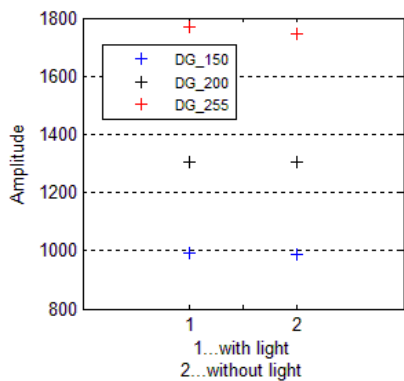


Figure 52 – *Amplitudes, dark grey target*

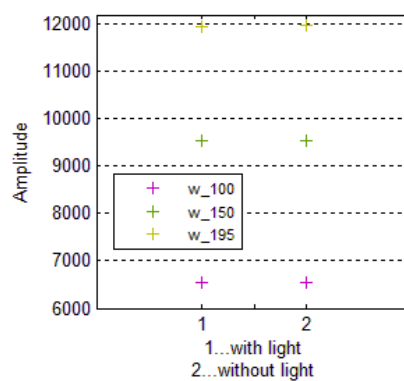


Figure 53 – *Amplitudes, white target*

The variations in the amplitude values caused by turning off the background light are minimal for both targets and can hence be disregarded.

Also the standard deviations impart the same conclusion (see figures 54 and 55). The changes are very small and can thus be assumed to be unimportant. The amplitudes in figure 53 are substantially higher than the values in figure 52, while the standard deviations in figure 55 are much lower than the comparable values in figure 54. This shows once more the differences in the returning amounts of energy depending on the reflectance of the material. Higher reflectance automatically means more energy and furthermore better quality of the obtained amplitude data.

The amplitude results of the dark grey target with an integration time of 150 ($\cong 15.3$ ms) in figure 54 compared with the results of the white target with the same integration time in figure 55 show again, that the amplitude values are in the same proportion as the reflectivity.

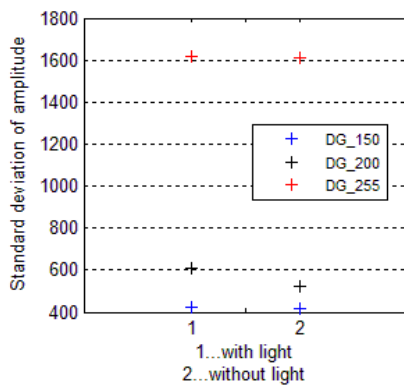


Figure 54 – *Standard deviations of amplitudes, dark grey target*

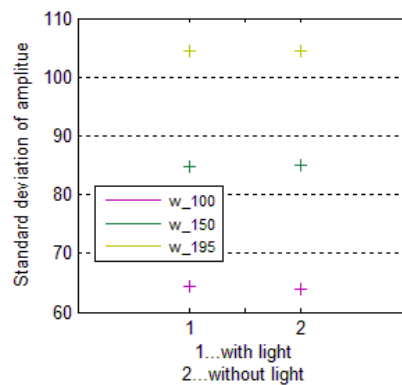


Figure 55 – *Standard deviations of amplitudes, white target*

4.6 Analysis of the Reference Survey

As already announced in 3.1.3, the distances measured with the range camera compared with the distances determined with the total station (reference distances) are the focus of the following section.

After (or simultaneously with) each of the four tests a reference survey was accomplished to determine precisely the distances between range camera and target. The measuring procedures have already been described in detail in section 3.1.3.

As most of the reference data was acquired during the Distance test, the according outcomes are illustrated first. Figure 56 shows the differences of distances determined with the SR4000 respectively the reference distances with increasing distance. The data is limited to the distances of 1.2m–4.6m, though, as the indoor-setup of the total station did not allow shorter distances than 1.2m. Larger distances were not included as the camera does not determine reliable results here anyway (see 2.3). In accordance with the Distance test (see section 4.3), the differences regarding each target and integration time are plotted.

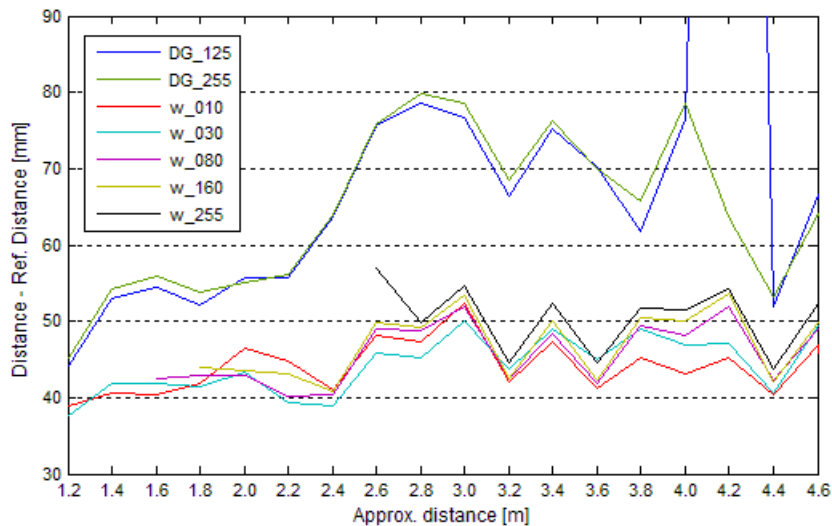


Figure 56 – Differences between the distances measured with the SR4000 and the reference distances determined with the total station, based on the Distance test

The differences between the distances from the range camera and the reference distances amount to 4-5 cm with the white target. Figure 56 also shows once more that objects with higher reflectivity lead to better distance results as the differences with the dark grey target are 1–2 cm higher on average and can even reach a value of 8 cm. However, distances determined with the SR4000 are longer than distances measured with a total station.

The jump of the blue graph (dark grey target, integration time of 125 ($\hat{=}$ 12.8 ms)) at a distance of 4.2 m is the already detected random error of mea-

surement (compare to figure 30).

The distance differences based on the Integration Time test and the Background Light test are illustrated together in figure 57. Regarding the Integration Time test, the differences of both targets and distances are plotted with increasing integration time. As the observed distances in the Background Light test and the Integration Time test were approximately the same (~ 1 cm difference), the distance differences of both tests can now be compared in figure 57. Regarding the Background Light test only one distance per target was used, though.

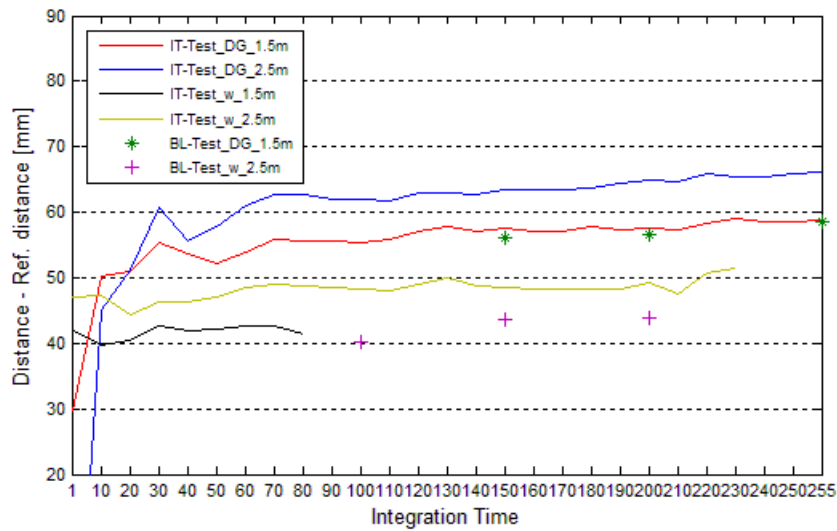


Figure 57 – Differences between the distances measured with the SR4000 and the reference distances determined with the total station, based on the Integration Time test and Background Light test

The resulting differences between distances measured with the range camera respectively with the total station in figure 57 are similar to the detected distances in figure 56. The values vary from 4-7 cm, depending on reflectivity and distance. Hence, a consistency of about 80% between the results of figure 56 and figure 57 can be recognized.

The results of the integration time data and the background light data in figure 57 show a good conformity too. In general, it is stated that the reflectivity is the strongest factor influencing the magnitude of the distance differences as high reflectivity leads to higher measurement accuracy. The integration time has only a small impact on the differences while increasing distances lead to higher distance differences by tendency.

As already noticed in section 4.4.1, the increasing drift of the dark grey target's graphs is also recognizable in figure 57. Hence, it can be stated that the systematic errors with the dark grey target rise slightly with increasing integration time.

In comparison with the Distance test, the Integration Time test and the Background Light test, the method of gathering reference data was different in the Warm Up test (see section 3.2.4). Thus, a comparison of the distance differences gathered with the Warm Up test would be pointless and hence is not addressed here.

5 Conclusion

In this thesis a performance evaluation of a range camera SR4000 was accomplished. Four different tests were performed to investigate the effect of several factors of influence on the range camera: The warm up time, the distance between camera and object of interest, the integration time and the background light. In addition, reference distances were measured with a total station during each test, and the resulting distances were compared with the distances measured with the range camera.

The Warm Up test dealt with the camera's performance during the warm up process. Basically, the distance increases during the warm up. The sharpest increase takes place within the first 10 minutes, though. The process of warming up can be modelled with an exponential function. Based on this function it can be stated that after 5 minutes the distance lies within the accuracy of ± 10 mm, which is specified as "absolute accuracy" by the manufacturer (99% reflectivity required). Generally, the number of invalid measurements decreases with the warm up time. Hence, it can be said that a longer warm up time leads to more reliable measurements.

The amplitudes never tended to a value within the first 50 minutes of operation. The parameters of a function modelling the amplitude distribution and also the standard deviation of the amplitudes showed that after 29 minutes the differences of amplitudes are independent from the warm up process but amplitudes as absolute measures are not independent even after 50 minutes of warming up.

The Distance test showed that the precision of distance measurements does not only depend on the distance between camera and object but also on the chosen integration time and the object reflectivity. A functional model was developed to predict the accuracy of distance measurements. Based on this model the standard deviations of the gathered distance data were normalized in further consequence in order to determine the occurring proportionality factor. It was also found out that the maximum distance of 5 m should not be exhausted to the full limit because the camera did not deliver reliable results even at a distance which was a few mm shorter than 5 m. In addition, two different modes of investigating the standard deviations were tested. The first mode based on the investigation of one pixel in each of 19 frames before the least squares adjustment, was more effective than the second mode (based on the standard deviation a posteriori of each single frame).

The amplitudes do not change remarkably with increasing distance. A normalization of the amplitudes with the integration time and the reflectivity

was accomplished and the results were consistent.

It is very important to choose a proper integration time. This fact was shown with the Integration Time test. Too much noise with low integration times and overexposure with too high integration times easily cause unreliable data. The effect of increasing integration time is strongly linked to the reflectivity. Regarding the acquired distance data, high reflectivity has only a minimal impact (changes in a range of a few mm) while low reflectivity causes higher variations. The standard deviations of the distance measurements showed that the increase of the integration time has no further effect as soon as a certain integration time is reached. The reason for this are systematic errors which start to dominate the results. Similar to the Distance test, the standard deviations of the distance measurements have been normalized according to the stated equation and the result confirmed the distance accuracy formula derived.

The standard deviations of amplitudes respectively the amplitudes themselves showed an almost perfect linearity to the integration time. It is also evident how much the reflectivity affects the amplitude measurements and their standard deviations. The slope of the linearity increases remarkably with decreasing reflectivity. The proportionality between the amplitude and the standard deviation of amplitude was also verified.

Background light causes a constant error of a few mm in the distance measurements, mostly depending on integration time and reflectivity. The effect of background light on the accuracy of distance measurements is negligible, though. Objects with high reflectivity are more robust against background light than objects with low reflectivity. The analysis of the amplitude measurements also supports the deduced distance accuracy formula.

The analysis of the reference survey showed that distances measured with the range camera are too long in terms of a few cm. It was also detected that especially lower reflectivity leads to longer distances but independently of integration time. Distance measurements with a 10%–reflectivity compared with measurements with a 99%–reflectivity showed consistently 1 cm difference or more.

5.1 Future Work

As some conclusions could not be drawn in this thesis because of too limited data acquisition, the recommendations for future work are mainly more ex-

tensive tests with the SR4000. Regarding the warm up time it is suggested to accomplish another Warm Up test over a longer period of time. It would be interesting to know if the amplitudes ever tend to a value at a certain point of time. Concerning the Distance test one suggestion would be to perform a similar test with either a larger target or a plain white wall. Due to the size of the target the applicable image sections were getting very small at longer distances here. Larger image sections or even a wall would hence lead to more usable data. A general recommendation is a higher number of frames to achieve higher over determination.

References

- [1] P. J. Besl. Active, Optical Range Imaging Sensors. *Machine Vision and Applications*, 1(2):127–152, 1988.
- [2] Bureau International des Poids et Mesures. *Le système international d'unités*. STEDI MEDIA, 2006.
- [3] B. Büttgen, T. Oggier, M. Lehmann, R. Kaufmann, and F. Lustenberger. CCD/CMOS Lock-In Pixel for Range Imaging: Challenges, Limitations and State-of-the-Art. Technical report, Swiss Center for Electronics and Microtechnology (CSEM), 2005.
- [4] F. Chiabrando, R. Chiabrando, D. Piatti, and F. Rinaudo. Sensors for 3D imaging: Metric Evaluation and Calibration of a CCD/CMOS Time-of-Flight Camera. *Sensors*, 9(12):10080–10096, 2009.
- [5] M. Frank, M. Plaue, H. Rapp, U. Köthe, B. Jähne, and F. A. Hamprecht. Theoretical and experimental error analysis of continuous-wave time-of-flight range cameras. *Optical Engineering*, 48:013602–1 – 013602–16, 2009.
- [6] H. Heinol. *Untersuchung und Entwicklung von modulationslaufzeit-basierten 3D-Sichtsystemen*. PhD thesis, University of Siegen, 2001.
- [7] B. Hofmann-Wellenhof, H. Lichtenegger, and J. Collins. *GPS Theory and Practice*. Springer, 1997.
- [8] T. Kahlmann. *Range Imaging Metrology: Investigation, Calibration and Development*. PhD thesis, University of Hannover, 2007.
- [9] T. Kahlmann, F. Remondino, and H. Ingensand. Calibration for increased accuracy of the range imaging camera SwissrangerTM. In *IS-PRS Comission V Symposium 'Image Engineering and Vision Metrology'*, 2006.
- [10] T. Kahlmann, F. Remondino, and S. Guillaume. Range imaging technology: new developments and applications for people identification and tracking. In *Proc. of Videometrics IX - SPIE-IS&T Electronic Imaging*, volume 6491, 2007.
- [11] W. Karel. Range Imaging: 3D-Punktwolken in Echtzeit. *VGI, Österreichische Zeitschrift für Vermessung und Geoinformation*, pages 15–26, 2007.

- [12] W. Karel, S. Ghuffar, and N. Pfeifer. Quantifying the distortion of distance observations caused by scattering in time-of-flight range cameras. In *The International Archives of Photogrammetry, Remote Sensing and Spatial Information Sciences. Vol. XXXVIII. Part 5*, 2010.
- [13] Koninklijke Philips Electronics N.V. Philips f32t8/tl835 series. Website. http://www.ecat.lighting.philips.com/1/catalog/catalog.jsp;jsessionid=29ABA8FB8749C621BD15F14D43633FB7.app106-drp3?ctn=927870083515_NA&productid=927870083515_NA_CA_LP_PROF_ATG&categoryid=LP_CF_F_T8COAT_EU_FA_CA_LP_PROF_ATG&title=F32T8%2FTL835+ALTO+TG+1LP&catalogType=LP_PROF_ATG&userLanguage=en&userCountry=ca&requestid=71263, pageview November 6th, 2011.
- [14] K. Kraus. *Photogrammetrie*. Walter de Gruyter, 2004. Band 1, Geometrische Informationen aus Photographien und Laserscanneraufnahmen.
- [15] K. Kraus and W. Schneider. *Fernerkundung*. Ferd. Dümmlers Verlag, 1988. Band 1, Physikalische Grundlagen und Aufnahmetechniken.
- [16] Labsphere Inc. Spectralon reflectance material. Website, 2011. http://www.pro-lite.co.uk/File/spectralon_material.php; pageview March 18th, 2011.
- [17] R. Lange. *3D Time-of-Flight Distance Measurement with Coustom Solid-State Image Sensors in CMOS/CCD-Technology*. PhD thesis, University of Siegen, 2000.
- [18] S. May, B. Werner, H. Surmann, and K. Pervözl. 3D Time-of-flight Cameras for Mobile Robotics. In *IEEE/RSJ International Conference on Intelligent Robots and Systems*, 2006.
- [19] Mesa Imaging. *SR4000 User Manual*, 2011. Version 2.0.
- [20] Mesa Imaging. Homepage of Mesa Imaging. Website, 2011. <http://www.mesa-imaging.ch>; pageview March 20th, 2011.
- [21] T. Möller, H. Kraft, J. Frey, M. Albrecht, and R. Lange. Robust 3D Measurement with PMD Sensors. Technical report, PMDTechnologies, 2005.
- [22] C. Netramai, M. Oleksandr, C. Joochim, and H. Roth. Motion Estimation of a Mobile Robot Using Different Types of 3D Sensors. In *IEEE*

- 4th International Conference on Automatic and Autonomous Systems*, 2008.
- [23] T. Oggier, M. Lehmann, R. Kaufmann, M. Schweizer, M. Richter, P. Metzler, G. Lang, F. Lustenberger, and N. Blanc. An all-solid state optical range camera for 3D real-time imaging with sub-sentimeter depth resolution (SwissRangerTM). Technical report, Swiss Center for Electronics and Microtechnology (CSEM), 2004.
- [24] T. Oggier, B. Büttgen, F. Lustenberger, G. Becker, B. Rüegg, and A. Hodac. SwissRanger SR3000 and first Experiences based on Miniaturized 3D-TOF Cameras. Technical report, Swiss Center for Electronics and Microtechnology (CSEM), 2005.
- [25] T. Pattinson. Quantification and description of distance measurement errors of a time-of-flight camera. Master’s thesis, University of Stuttgart, 2010.
- [26] H. Ruser. *Ultraschall-Mikrowellen-Sensorsystem zur Geschwindigkeits- und Abstandsmessung mit diversitär-redundanter Auswertung der Phasensignale*. PhD thesis, Universität der Bundeswehr München, 2003.
- [27] R. Schwarte, H. Heinol, B. Buxbaum, T. Ringbeck, Z. Xu, and K. Hartmann. *Handbook of Computer Vision and Applications*, chapter Principles of Three-Dimensional Imaging Techniques, pages 463–484. Academic Press, 1999.
- [28] W. Schwarz. Vermessungen im Sub-Millimeter-Bereich. *DVW Bayern Mitteilungen*, pages 584–608, 2006.
- [29] O. Steiger, J. Felder, and S. Weiss. Calibration of Time-of-Flight Range Imaging Cameras. In *15th IEEE International Conference on Image Processing*, 2008.
- [30] S. Vacek, T. Schamm, J. Schröder, and R. Dillmann. Collision Avoidance for Cognitive Automobiles Using a 3D PMD Camera. In *IFAC Symposium on Intelligent Autonomous Vehicles*, 2007.
- [31] C. A. Weyer, K.-H. Bae, K. Lim, and D. D. Lichti. Extensive Etrinsic Performance Evaluation of a 3D Range Camera. In *The International Archives of Photogrammetry, Remote Sensing and Spatial Information Sciences. Vol. XXXVII. Part B5*, 2008.
- [32] H. Zetsche. *Elektronische Entfernungsmessung (EDM)*. Wittwer, 1979.

List of Figures

1	Overview of contact-less 3D measurements	4
2	Setup of a triangulation	5
3	Pulse Modulation	6
4	Continuous Wave Modulation	7
5	Phase shift measurement principle	8
6	Swiss Ranger SR4000	10
7	Typical measurement setup	13
8	White Spectralon target	14
9	Dark grey Spectralon target	14
10	<i>Mesa Imaging</i> Demo Software	16
11	Camera's offset	18
12	Target's offset	19
13	Temporal change of measured distances	24
14	Temporal change of amplitudes	24
15	Comparison of reference- and measured distances	28
16	Variations in range results at ~ 3.4 m	29
17	Distance measurements depending on the integration time, ~ 1.5 m	31
18	Distance measurements depending on the integration time, ~ 2.5 m	32
19	Setup for the Background Light test	35
20	Distance with and without background light, dark grey target	36
21	Distance with and without background light, white target . . .	36
22	Example of a fitting plane	38
23	Example of a fitting paraboloid	39
24	Temporal change of distances in the analysis	41
25	Modelled process of warming up	42
26	Temporal change of amplitudes in the analysis	43
27	Trend of the adjusted parameters of the paraboloid	44
28	Standard deviation of the amplitudes	45
29	Number of measurements with increasing distance	46
30	Comparison between reference and measured distances, based on the adjusted data	47
31	Standard deviations of 19 frames, based on the middle pixel .	48
32	Standard deviations of 19 frames, based on the middle pixel .	50
33	Normalized standard deviations, dark grey target	50
34	Normalized standard deviations, white target	50
35	Normalized standard deviations, 0.6–2.0 m	51
36	Normalized standard deviations, 2.0–3.4 m	51

37	Normalized standard deviations, 3.4–4.8 m	51
38	Frequency distribution of the normalized standard deviations .	51
39	Standard deviations a posteriori for each frame, based on the middle pixel	52
40	Amplitudes, based on the middle pixel	53
41	Normalized Amplitudes	54
42	Distance measurements depending on the integration time, based on the middle pixel, ~ 1.5 m	55
43	Distance measurements depending on the integration time, based on the middle pixel, ~ 2.5 m	55
44	Standard deviations of the distance measurements a posteriori	56
45	Frequency distribution of the normalized standard deviations .	57
46	Amplitudes - based on the middle pixel - and standard deviation of amplitudes a posteriori, dark grey target	58
47	Amplitudes - based on the middle pixel - and standard deviation of amplitudes a posteriori, white target	59
48	Distance measurements after adjustment, dark grey target . .	60
49	Distance measurements after adjustment, white target	60
50	Standard deviations, dark grey target	61
51	Standard deviations, white target	61
52	Amplitudes, dark grey target	61
53	Amplitudes, white target	61
54	Standard deviations of amplitudes, dark grey target	62
55	Standard deviations of amplitudes, white target	62
56	Distance – Reference distance, Distance Test	63
57	Distance – Reference distance, Integration Time test and Back- ground Light test	64

List of Tables

1	Variables of the Warm Up test, white target	22
2	Variables of the Distance test	27
3	Variables of the Integration Time test	30
4	Variables of the Background Light test, dark grey target . . .	34
5	Variables of the Background Light test, white target	34

A Appendix

A.1 Datasheet Range Camera SR4000

SR4000 Data Sheet



MESA
IMAGING

1 Product Specifications

Standard Field of View Cameras (43° (h) x 34° (v)) and Wide Field of View Cameras (69° (h) x 56° (v))					
Product Number	00400001	00400002	00400006	00400009	Standard Field of View Cameras (43° (h) x 34° (v))
	00400014	00400011	00400015	00400013	Wide Field of View Cameras (69° (h) x 56° (v))
Communication interface	USB	Fast Ethernet	USB	Fast Ethernet	
Modulation Frequency	29/30/31 MHz		14.5/15/15.5 MHz		Frequency selectable, allows multiple cameras to operate simultaneously
Non Ambiguity Range	5.0 m		10.0 m		Ranges are radial distances, not z distances
Calibrated Range	0.8 to 5.0 m		0.8 to 8.0 m		For 15 MHz: values from 8 - 10 m are extrapolated, not calibrated ¹
Absolute accuracy ⁽³⁾	+/-10 mm (typ.)		+/-15 mm (typ.)		At 99% target reflectivity, over calibrated range ^{1,2}
Drift with temperature (T)	$\leq 0.5 \text{ mm}/^{\circ}\text{C}$ (max) $\leq 1.5 \text{ mm}/^{\circ}\text{C}$ (max.)				For $20^{\circ}\text{C} \leq T \leq 30^{\circ}\text{C}$ For $10^{\circ}\text{C} \leq T \leq 50^{\circ}\text{C}$
Repeatability (1 σ) of central pixels ⁽²⁾	4 mm (typ.) 7 mm (max.)		6 mm (typ.) 9 mm (max.)		At 99% target reflectivity, 30 FPS, 2 m working distance. ^{1,4}
Repeatability (1 σ) in Region 1	$\sigma \leq 120\%$ of maximal value for central pixels				Measurement regions are defined in section 1.1
Repeatability (1 σ) in Region 2	$\sigma \leq 200\%$ of maximal value for central pixels				Measurement regions are defined in section 1.1

(1) All values are indicated for 30 MHz or 15 MHz respectively. Values at adjacent frequencies (14.5, 15.5 and 29, 31 MHz) will differ slightly

(2) For 11 x 11 central pixels of the camera

(3) Includes drift induced by changing integration times

(4) Typical: @ 25°C. Max: over complete temperature range (+10 °C to +50 °C)

1.1 Definition of measurement regions

Measurement regions: definition Region 1: Dark red Region 2: Bright red	Measurement regions: polar dimensions Region 1: $\pm 17^{\circ}$ Region 2: $\pm 27^{\circ}$
Measurement regions: representation over pixel field Standard field of view cameras (43° (h) x 34° (v))	Measurement regions: representation over pixel field Wide field of view cameras (69° (h) x 56° (v))

2 General Specifications (standard and wide field of view cameras)

Imager parameters (z)	Value	Comment
Illumination Wavelength	850 nm	Central wavelength
Optical filter	-	Bandpass / Glass substrate
Maximum Frame Rate	50 FPS	Camera setting dependent

Imager parameters (x,y)	Value	Comment
Pixel Array Size	176 (h) x 144 (v)	QCIF
Field of View	43.6° (h) x 34.6° (v) or 69° (h) x 56° (v)	Standard field of view cameras Wide field of view cameras
Pixel Pitch	40 µm	Horizontal and vertical
Angular Resolution	0.24° 0.39°	Standard field of view; central pixels Wide field of view; central pixels
Focus length / adjustment	10 mm 5.8 mm	Standard field of view cameras Wide field of view cameras Manually adjustable over operating range

Environmental	Value	Comment
External light disturbances	Designed for indoor use	Not to be used in direct sunlight
Operating Temperature	+10 °C to +50 °C (50 °F to 122 °F)	Housing temperature
Storage Temperature	-20 °C to +70 °C (-4 °F to 158 °F)	

Power Connections	Value	Comment
Electrical Power Requirements	12 V (-2%; +10%), maximum 1.0 A, (typical 0.8 A)	Power supply available from MESA
Trigger connector	Lumberg M8 Male 4-pin	Screw connector (on camera)
Power connector	Lumberg M8 Male 3-pin	Screw connector (on camera)

Software	Value	Comment
Software Drivers	Windows XP, Windows 7 (32-bit and 64-bit), Vista (32-bit and 64-bit), Linux 32-bit	
Software API	C, C++, Matlab	

Software features	Value	Comment
Modulation frequency selection	29/30/31 MHz or 14.5/15/15.5 MHz selectable	Depending on camera model
Acquisition mode	Continuous, Triggered	Trigger via Software or Hardware
Integration time	0.3 to 25.8 ms, steps of 0.1 ms	Selectable
Confidence Map	Measures quality of distance data, quality threshold to be set by user	

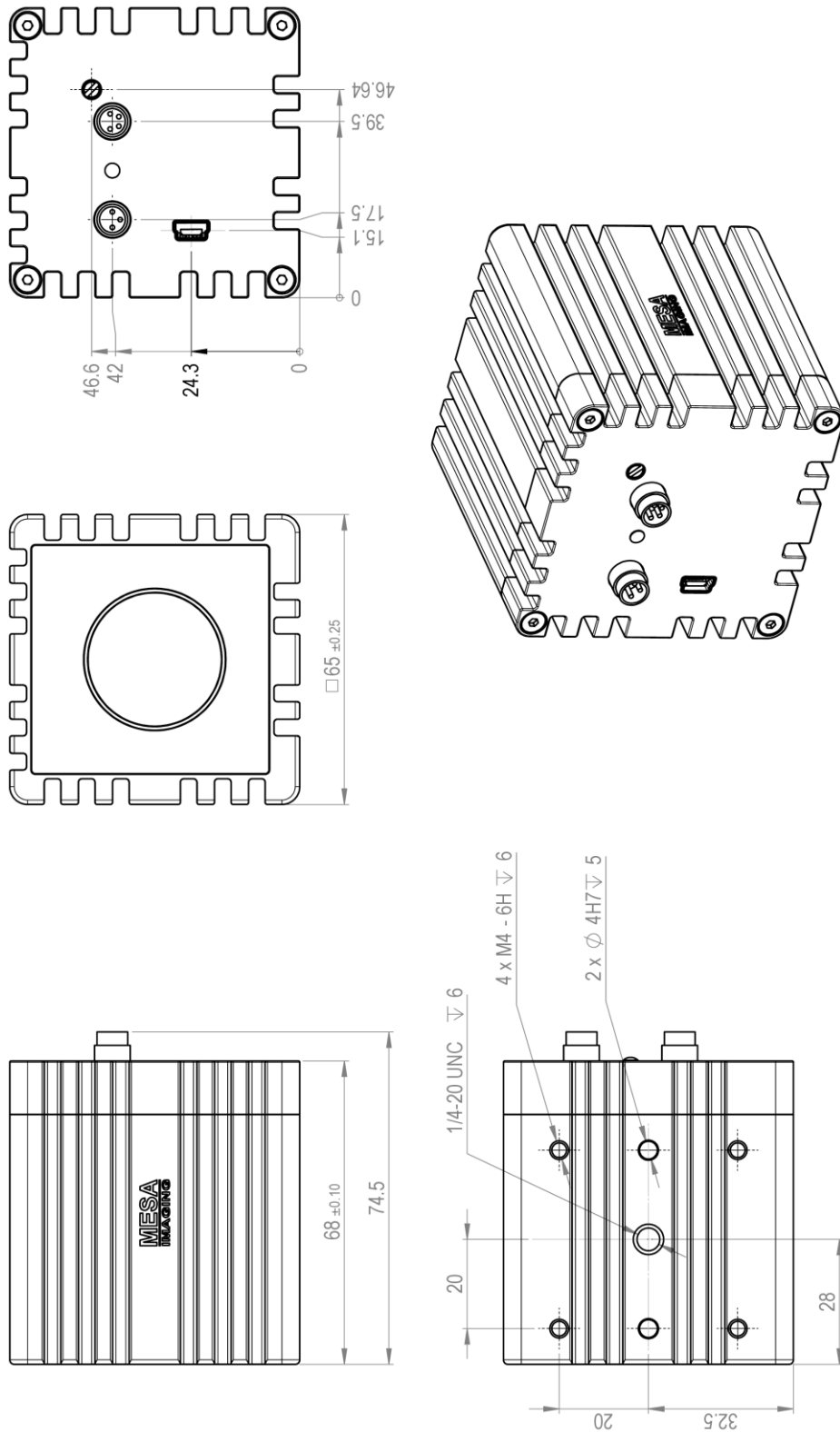
Data output	Value	Comment
Spherical distance (Range)	0-65535 (16 Bit) <--> 0-5 m 0-65535 (16 Bit) <--> 0-10 m	@ 30 MHz modulation @ 15 MHz modulation Data output from camera without Cartesian coordinate transfer
Cartesian XYZ coordinates	x, y, z (m)	Up to 5 m distance @ 30 MHz modulation Up to 10 m distance @ 15 MHz modulation
Signal amplitude	0-65535 (16 Bit)	Value above 32767 indicates saturation
Converted grayscale Image	0-65535 (16 Bit)	Value above 32767 indicates saturation
Confidence Map	0-65535 (16 Bit)	Quality threshold to be set by user

Ratings	Value	Comment
Enclosure rating	IP 40	
Eye safety	EN 60825-1: 2002: Class 1	
EMC	EN 55022 : Class A EN 61000 EN 55024	

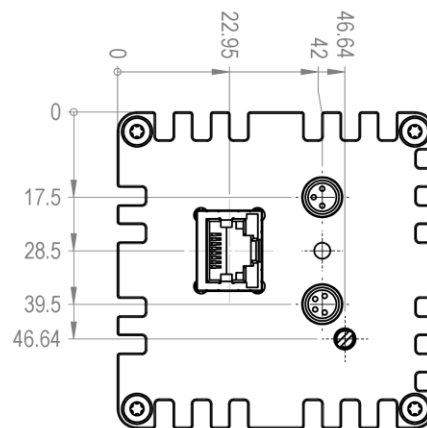
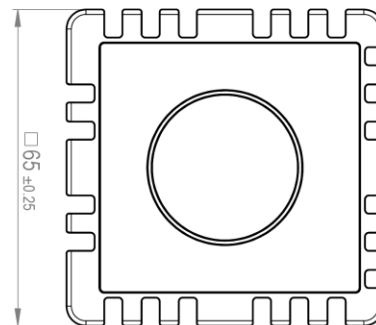
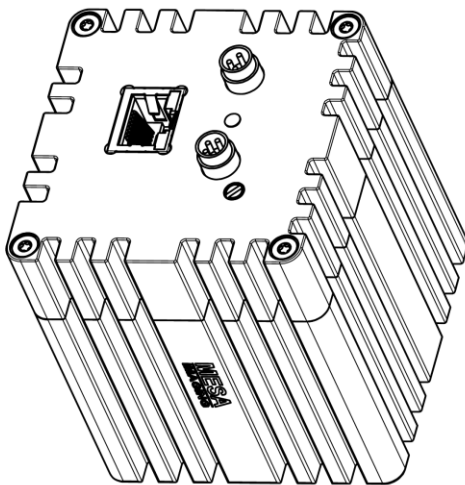
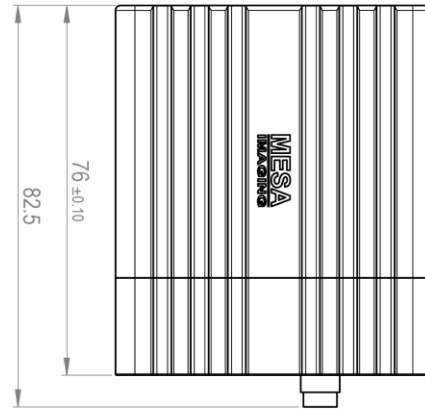
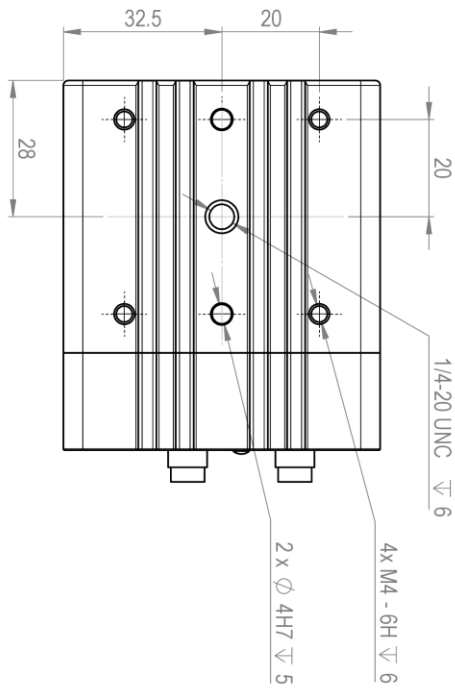
Mechanical	Value	Comment
Dimensions	65 x 65 x 68 mm 65 x 65 x 76 mm	For USB cameras For Ethernet cameras Excludes the connectors
Case Material	Anodized Aluminum	
Color front housing	Black	
Color back cover	Red	
Window Material	Polycarbonate	Illumination cover
	Borofloat glass	Objective cover
Mounting Holes	4 x M4; 2 x 4H7; 1 x 1/4"	
Weight	470 g 510 g	For USB cameras For Ethernet cameras
Cooling	Passive, no fan	Camera always to be connected to a heat sink

3 Mechanical

3.1 Camera Dimensions and Mounting - USB cameras (00400001, 006, 014 and 015)

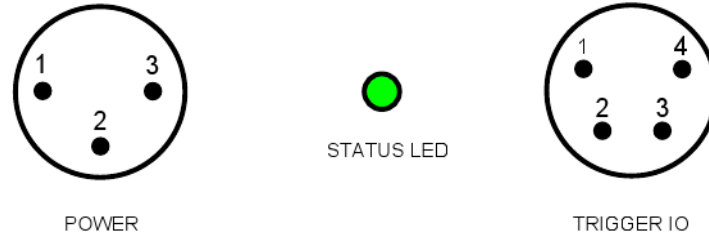


3.2 Camera Dimensions and Mounting - Ethernet cameras (00400002, 009, 011 and 013)



3.3 Camera power and trigger connectors

- Schematic view of the connectors on the backplane of the camera -



Detailed description on the pin's functions is given in the next two paragraphs.

The camera also includes a status LED. Regular pulsing of the status LED indicates that the camera is powered; fast pulsing of the status LED indicates data transfer between camera and computer.

3.3.1 Power requirements

- Power Connections -

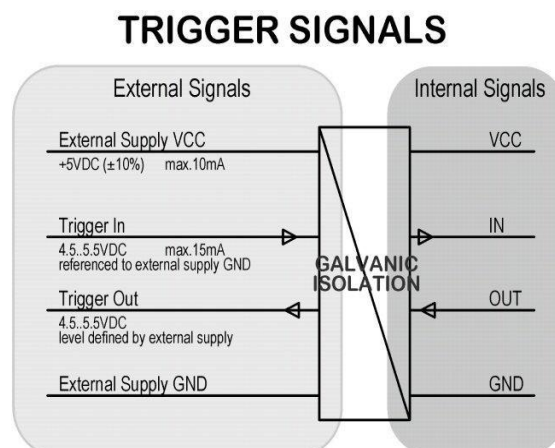
1	+12 VDC; min -2%; max +10%	Typ. 0.8 A @ 12 V, min 0.6 A , max 1.0 A
2	SHIELD	Connect to earth
3	GND	

3.3.2 Trigger requirements

- Trigger I/O Connections -

1	External Voltage	4.5 - 5.5 V / 10 mA - defines the logic level of the trigger output
2	Trigger In	4.5 - 5.5 V / 15 mA - Start acquisition frame
3	Trigger Out	4.5 - 5.5 V - Frame ready to fetch
4	External GND	In reference to External Voltage

- Schematic view of the hardware trigger logic -



3.4 Declaration of CE conformity

Declaration of CE conformity

The undersigned, representing the following manufacturer

MESA Imaging AG
Technoparkstrasse 1
8005 Zürich
Switzerland

Herewith declare that the products:

SR 00400001	Hardware version 2.0 and higher
SR 00400002	Hardware version 2.0 and higher
SR 00400006	Hardware version 2.0 and higher
SR 00400009	Hardware version 2.0 and higher
SR 00400011	Hardware version 2.0 and higher
SR 00400013	Hardware version 2.0 and higher
SR 00400014	Hardware version 2.0 and higher
SR 00400015	Hardware version 2.0 and higher

have been tested and are in conformity with the following CE directives for industrial environments:

Eye Safety	EN 60825-1: 2002	Class 1
EMC	EN 55022	Class A
EMC	EN 55024	
EMC	EN 61000-6-1	
EMC	EN 61000-6-2	
EMC	EN 61000-6-4	

Therefore the above mentioned products are in conformity with all CE directives relating to industrial environments.

Zürich

4th of June, 2010


.....
James Lewis
CEO

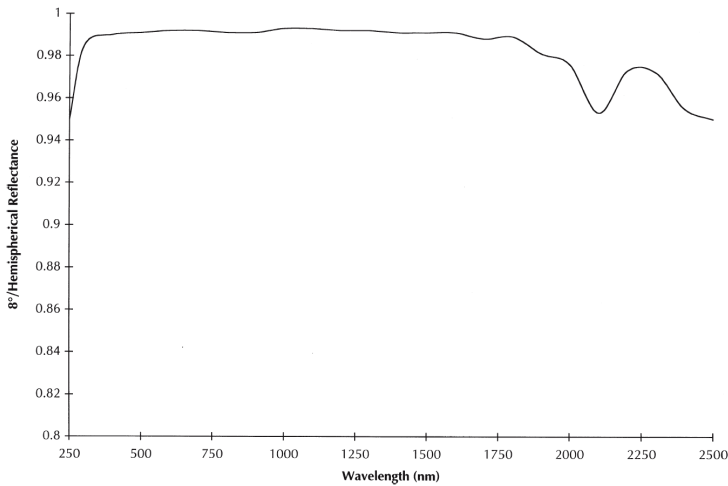

.....
Christian Waizenegger
Product Manager

A.2 Datasheet Spectralon Targets

DIFFUSE REFLECTANCE TARGETS

Durable reflectance panels for laboratory and field applications that require exposure to harsh conditions

TYPICAL 8° HEMISPHERICAL REFLECTANCE - SRM-990



SPECTRALON® TARGETS

Spectralon targets are ideal for laboratory and field applications that require long exposure to harsh environmental conditions such as field validation experiments performed to collect remote sensing data. Because of the diffuse reflectance properties of Spectralon, these targets maintain a constant contrast over a wide range of lighting conditions.

Spectralon targets are available in plates up to 24 inches square and are available in white or gray material and are mounted in a rugged anodized aluminum frame. Calibration data from 250 to 2500nm, every 50nm is supplied with the targets. Calibration data is traceable to the National Institute of Standards and Technology (NIST). All targets are thermally and chemically stable and easily cleaned. Targets larger than 24 inches squared can be constructed and calibrated, custom targets of various reflectance values are also available up to 3 meters squared.

FEATURES:

- Durable and washable
- High reflectance
- Impervious to harsh environments
- Diffuse reflectance

APPLICATIONS:

- Backlight Illuminators
- Environmental Test Targets
- Laser Targets
- Optical Reflectors
- Remote Sensing Targets

SPECTRALON® CONTRAST TARGETS

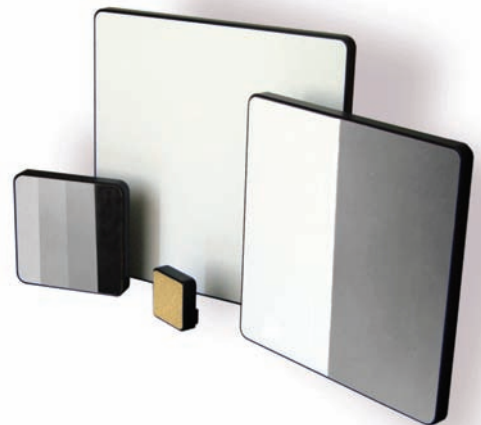
Spectralon Contrast Targets are perfect for the calibration of video cameras, densitometers, the contrast transfer of propagation media, and the testing of imaging systems in field conditions.

These chemically inert targets are durable and washable, consisting of a diffuse white (99% reflectance) and a diffuse dark gray (10% reflectance) panel mounted side-by-side in an anodized aluminum frame.

Spectralon multi-step targets consist of four panels of 99, 50, 25 and 12% reflectance values mounted side-by-side. The four panels provide equal optical density differences and equal contrast between each adjacent panel.

INFRAGOLD® TARGETS

Infragold® targets are mounted in an anodized aluminum frame and are used for infrared applications. Targets are available in plates up to 18 inches square. Larger infrared targets can be constructed and calibrated by arranging Infragold plates in arrays; seams may be visible but do not affect the overall reflectance of the target.



Specifications

Spectralon® Diffuse Reflectance Targets

Target part no.	Reflectance Value	Reflective Area (inches)	Size Mounted (LxWxH inches)	Order Number
SRT-02-020	2%	2 x 2	2.25 x 2.25 x 0.56	AA-00823-900
SRT-02-050	2%	5 x 5	5.25 x 5.25 x 0.56	AA-00821-900
SRT-02-100	2%	10 x 10	10.25 x 10.25 x 0.56	AA-00822-900
SRT-02-120	2%	12 x 12	12.25 x 12.25 x 0.56	AA-00827-900
SRT-02-180	2%	18 x 18	18.25 x 18.25 x 0.56	AA-00826-900
SRT-02-240	2%	24 x 24	24.25 x 24.25 x 0.56	AA-00837-900
SRT-05-020	5%	2 x 2	2.25 x 2.25 x 0.56	AA-00823-800
SRT-05-050	5%	5 x 5	5.25 x 5.25 x 0.56	AA-00821-800
SRT-05-100	5%	10 x 10	10.25 x 10.25 x 0.56	AA-00822-800
SRT-10-020	10%	2 x 2	2.25 x 2.25 x 0.56	AA-00823-700
SRT-10-050	10%	5 x 5	5.25 x 5.25 x 0.56	AA-00821-700
SRT-10-100	10%	10 x 10	10.25 x 10.25 x 0.56	AA-00822-700
SRT-20-020	20%	2 x 2	2.25 x 2.25 x 0.56	AA-00823-600
SRT-20-050	20%	5 x 5	5.25 x 5.25 x 0.56	AA-00821-600
SRT-20-100	20%	10 x 10	10.25 x 10.25 x 0.56	AA-00822-600
SRT-40-020	40%	2 x 2	2.25 x 2.25 x 0.56	AA-00823-500
SRT-40-050	40%	5 x 5	5.25 x 5.25 x 0.56	AA-00821-500
SRT-40-100	40%	10 x 10	10.25 x 10.25 x 0.56	AA-00822-500
SRT-50-020	50%	2 x 2	2.25 x 2.25 x 0.56	AA-00823-400
SRT-50-050	50%	5 x 5	5.25 x 5.25 x 0.56	AA-00821-400
SRT-50-100	50%	10 x 10	10.25 x 10.25 x 0.56	AA-00822-400
SRT-50-120	50%	12 x 12	12.25 x 12.25 x 0.56	AA-00827-400
SRT-50-180	50%	18 x 18	18.25 x 18.25 x 0.56	AA-00826-400
SRT-50-240	50%	24 x 24	24.25 x 24.25 x 0.56	AA-00837-400
SRT-60-020	60%	2 x 2	2.25 x 2.25 x 0.56	AA-00823-300
SRT-60-050	60%	5 x 5	5.25 x 5.25 x 0.56	AA-00821-300
SRT-60-100	60%	10 x 10	10.25 x 10.25 x 0.56	AA-00822-300
SRT-75-020	75%	2 x 2	2.25 x 2.25 x 0.56	AA-00823-200
SRT-75-050	75%	5 x 5	5.25 x 5.25 x 0.56	AA-00821-200
SRT-75-100	75%	10 x 10	10.25 x 10.25 x 0.56	AA-00822-200
SRT-75-120	75%	12 x 12	12.25 x 12.25 x 0.56	AA-00827-200
SRT-75-180	75%	18 x 18	18.25 x 18.25 x 0.56	AA-00826-200
SRT-75-240	75%	24 x 24	24.25 x 24.25 x 0.56	AA-00837-200
SRT-80-020	80%	2 x 2	2.25 x 2.25 x 0.56	AA-00823-100
SRT-80-050	80%	5 x 5	5.25 x 5.25 x 0.56	AA-00821-100
SRT-80-100	80%	10 x 10	10.25 x 10.25 x 0.56	AA-00822-100
SRT-99-020	99%	2 x 2	2.25 x 2.25 x 0.56	AA-00823-000
SRT-99-050	99%	5 x 5	5.25 x 5.25 x 0.56	AA-00821-000
SRT-99-100	99%	10 x 10	10.25 x 10.25 x 0.56	AA-00822-000
SRT-99-120	99%	12 x 12	12.25 x 12.25 x 0.56	AA-00827-000
SRT-99-180	99%	18 x 18	18.25 x 18.25 x 0.56	AA-00826-000
SRT-99-240	99%	24 x 24	24.25 x 24.25 x 0.56	AA-00837-000

Spectralon® Contrast Targets

Target Part No.	Type	Reflectance Values	Reflective area (inches)	Order Number
SRT-SP-050	Split	99, 10%	5 x 5	AA-00656-000
SRT-SP-100	Split	99, 10%	10 x 10	AA-00657-000
SRT-SP-180	Split	99, 10%	18 x 18	AA-00658-000
SRT-MS-050	Multi-step	99, 50, 25, 12%	5 x 5	AA-00659-000
SRT-MS-100	Multi-step	99, 50, 25, 12%	10 x 10	AA-00660-000
SRT-MS-180	Multi-step	99, 50, 25, 12%	18 x 18	AA-00661-000

Infragold® Diffuse Reflectance Targets

Target Part No.	Reflectance Value	Reflective Area (inches)	Size Mounted (inches)	Order Number
IRT-94-020	94%	2 x 2	2.25 x 2.25 x 0.31 T	AA-00026-121
IRT-94-050	94%	5 x 5	5.25 x 5.25 x 0.31 T	AA-00026-221
IRT-94-100	94%	10 x 10	10.25 x 10.25 x 0.31 T	AA-00026-320
IRT-94-180	94%	18 x 18	18.25 x 18.25 x 0.31 T	AA-00050-020



B Curriculum Vitae

Persönliche Daten

Name: Alexandra von Beringe
Anschrift: Görgengasse 23/3/6
1190 Wien
a.vonberinge@gmail.com
Eltern: Niklas von Beringe, Softwareentwickler (selbständig)
Dipl.-Päd. Sylvia von Beringe, VS-Lehrerin

Ausbildungsweg

Schulbildung: 4 Jahre Volksschule Flotowgasse, Wien
3 Jahre Bundesrealgymnasium Billrothstraße, Wien
5 Jahre Bundesrealgymnasium Krottenbachstraße, Wien
Studium: WS2004 - SS2012 Diplomstudium Vermessung und
Geoinformation an der Technischen Universität Wien,
Studienzweig Geodäsie und Geophysik
1. Diplomprüfung mit Auszeichnung im Jänner 2007
Auslandssemester an der University of Calgary, Kanada
im WS2009

Berufliche Erfahrungen

August 2006	MA41, Stadtvermessung
Dez. 2006 - Feb. 2007	Raumumwelt Planungs GMBH
August 2007	MA41, Stadtvermessung
Juli/August 2008	MA41, Stadtvermessung
Juni/Juli 2009	MA41, Stadtvermessung
August/Sept. 2010	MA41, Stadtvermessung
August 2011	MA41, Stadtvermessung
Nov./Dez. 2011	MA41, Stadtvermessung

Studienbezogenes Engagement

01.07.2005 - 30.06.2007	Studienvertreterin, Fachschaft Vermessung u. Geoinformation
01.07.2007 - 30.06.2009	Fachschaftsvorsitzende
21.05.2009 - 24.05.2009	73. ARGEOS - Treffen Wien (Hauptorganisation)
30.06.2010 - 07.07.2010	ISPRS Kongress Wien (Mitglied des Organisationsteams)